Self-healing capacity of mortars with added-in bio-plastic bacteria-based agents Characterization and quantification through micro-scale techniques

Roy, Rahul; Rossi, Emanuele; Silfwerbrand, Johan; Jonkers, Henk

DOI
10.1016/j.conbuildmat.2021.123793

Publication date
2021

Document Version
Final published version

Published in
Construction and Building Materials

Construction and Building Materials 297 (2021) 123793

Contents lists available at ScienceDirect

Construction and Building Materials

journal homepage: www.elsevier.com/locate/conbuildmat

Self-healing capacity of mortars with added-in bio-plastic bacteria-based agents: Characterization and quantification through micro-scale techniques

Rahul Roy [a,*], Emanuele Rossi [b], Johan Silfwerbrand [a], Henk Jonkers [b]

[a] Department of Civil and Architectural Engineering, Division of Concrete Structures, KTH Royal Institute of Technology, 100 44 Stockholm, Sweden
[b] Microlab, Section of Materials and Environment, Faculty of Civil Engineering and Geosciences, Delft University of Technology, 2628 CN Delft, The Netherlands

HIGHLIGHTS

- Bio-plastic healing agents are investigated for the self-healing efficiency of mortar specimens.
- Quantification and characterization of the self-healing by the healing agents are performed.
- Healing agents displayed better crack closure performance compared to plain mortar.
- Healing agents displayed better recovery of water tightness compared to plain mortar.
- Internal crack geometry governs the variability in the crack width and water flow.

ARTICLE INFO

Article history:
Received 28 January 2021
Received in revised form 7 May 2021
Accepted 27 May 2021

Keywords:
Bacteria
Healing agent
Alkanoate derivatives
Lactic acid derivatives
Self-healing
Statistical analysis

ABSTRACT

In this study, a novel non-toxic, biodegradable bacteria-based healing agent known as alkanoate derivatives (AKD) derived from wastewater was investigated for its self-healing efficiency of the mortar specimens in comparison to the already-developed healing agents made of lactic acid derivatives (PLA). Mortar with different percentages of healing agent inclusions (2.6% and 5% w/w cement) have been evaluated in this study. To assess the self-healing improvements of the mortar incorporated bacteria-based bio-plastic healing agent's self-healing capacity, quantification of self-healing efficiency was performed at two different healing intervals of 28 and 56 days through optical determination of crack closure by stereomicroscope, recovery of water tightness by rapid water permeability test and determination of mass percentage increase of calcium carbonate by thermogravimetric analysis (TGA). The healing products formed in the cracks were analyzed by TGA and X-ray diffraction (XRD). Furthermore, a statistical analysis was performed to understand the variability in the crack width, water flow and the correlation of self-healing ratios between the stereomicroscope and permeability measurements. The results revealed that series containing the healing agents displayed a higher crack closure ratio compared to plain mortar series for initial crack widths greater than 0.4 mm at 56 days of healing. Moreover, the recovery of water tightness for series containing bacteria were greater compared to plain mortar for initial crack widths greater than 0.6 mm at 56 days of healing. However, in healing agent incorporated mortar series, only alkanoate derivatives at 5% dosage reported an increase in mass % of calcium carbonate precipitation at 56 days of healing. From the statistical analysis, it was confirmed that the influence of internal crack geometry plays a significant role in the degree of healing and variation of the water flow for smaller crack widths as the healing period increases.

1. Introduction

Concrete is the most commonly used man-made construction material on the earth and cement is used to make about 2.5 metric tons (over one cubic meter) of concrete per human being alive per year [1]. It is a brittle material, relatively strong in compression but comparatively weak in tension and, thus vulnerable to cracking.

* Corresponding author.
E-mail addresses: rahulr@kth.se (R. Roy), e.rossi@tudelft.nl (E. Rossi), jsilfwer@kth.se (J. Silfwerbrand), h.m.Jonkers@tudelft.nl (H. Jonkers).

https://doi.org/10.1016/j.conbuildmat.2021.123793
0950-0618/

Cracks in the concrete are inevitable and occur not only due to the external mechanical loading but also as a result of chemical shrinkage, drying shrinkage or autogenous shrinkage [2]. These cracks hinder the durability of concrete since they offer a convenient route for the movement of liquids and gasses that potentially contain harmful substances. To keep concrete structures durable, it is necessary to control the crack width and to heal the cracks as soon as possible. Concrete structures require frequent and scheduled inspection for repair and maintenance, which are significantly time- and money-consuming. In Europe, approximately 50% of the annual construction budget has been estimated for reconstruction and renovation of existing facilities [3]. Self-healing of cracks in concrete thus leads to low maintenance costs and a longer service life of concrete structures [4–6]. However, the autogenous healing in concrete due to the cement hydration and carbonation of portlandite can effectively heal cracks only up to 0.2 mm [7].

Microbially induced carbonate precipitation (MICP) has been studied in recent decades as an environmentally friendly method for surface consolidation and preservation of decayed ornamental stones and concrete. The method was first applied to form a compatible and highly coherent carbonate precipitate on limestone. Later, this method was explored to improve the durability of cement-based materials. In addition, the same concept has also been extended to the generation of a biological binder [8–15]. Recent advances indicate the potential use of this technique for the remediation of cracks in building materials, strength improvement and self-healing of cementitious materials. The principle behind the MICP in self-healing concrete involves the application of mineral-producing bacteria (added-in as spores) which converts the organic carbon substrate to precipitate calcium carbonate onto the crack face in the concrete These bacterial spores are added in the fresh mixture with nutrients, organic carbon substrate and other repair agents. The spores remain dormant in the concrete matrix but can germinate as soon as cracks occur. As the concrete cracks, the bacteria start to proliferate after the ingress of water and oxygen through cracks and produces calcium carbonate on the crack faces through aerobic oxidation. As a result, the produced crystals will block cracks and cause cracks to self-repair. Efficient self-healing is done if the sealing is a long-term success and can be accomplished throughout the lifespan of a system. The survival of bacteria is therefore particularly important. However, there can be several barriers to the survival of bacteria when bio-agents are directly added to concrete. Research has shown that while bacterial spores have already been introduced, the lives of unencapsulated or non-immobilized spores are restricted to only two months, and therefore only young samples have been effectively self-healed [16]. This might have many causes including cement matrix alkalinity, concrete mixing, and cement hydration [16]. One way to tackle this constraint is to encapsulate the bacteria to protect them, without affecting bacteria's concrete properties and ability to precipitate calcium carbonate. Several methodologies have been reported in the current literature to encapsulate the healing agents (spores or combination of spores and nutrients) but not limited to the following, such as superabsorbent hydrogels [17–21], silica gel/polyurethane [22], melamine microcapsules [23], rubber particles [24], lightweight aggregates (LWA) [25–29], diatomaceous earth [30,31] and biochar [32,33]. According to Jonkers et al. [16], incorporation of healing agents in LWA substantially prolonged the lifetime of the bacterial spores in the concrete matrix. In some research studies [56–57], self-protected bacterial cultures have also been investigated. Moreover, the utilization of calcium lactate as an organic carbon substrate in the LWA had resulted in 10% increase in compressive strength in comparison to other organic carbon substrates such as calcium acetate, yeast extract and peptone [11]. However, due to the incorporation of LWA volumes, which influence the mixture design, the application range may be limited. To expand the application range by scaling the healing agent particles, Mors et al. [34,35] investigated an alternative healing agent (HA) additive which solely consists of bacterial spores, nutrients and organic carbon substrate made of lactic acid derivatives (PLA). This addition of HA (4% by weight of cement) reported three times enhanced cracked water tightness of the mortar [35] in comparison to the control series. Rodriguez et al. [36] carried out quantification studies of the tensile strength and elastic modulus in the interface zone (IZ) between the HA additives (0.6% and 1.3% by w/w) and the cement paste to understand the influence in terms of characteristics and dosage of these HA additives. Rossi et al. [37] investigated the self-healing capacity of these HA additives at 2.6% dosage and reported an improvement in the recovery of watertightness and 28 days compressive strength of the HA mortar composites in comparison to control series. These studies indicate that the incorporation of PLA in the HA additives can significantly improve the self-healing capacities due to the presence of calcium lactate ($Ca(C_3H_5O_3)_2$) which produces six equivalents of calcium carbonate ($CaCO_3$) and five equivalents of carbon dioxide from one equivalent of calcium lactate when undergoing aerobic oxidation, as described below [11].

$$Ca(C_3H_5O_3)_2 + 6O_2 \rightarrow CaCO_3 + 5CO_2 + 5H_2O \quad (a)$$

$$5CO_2 + 5Ca(OH)_2 \rightarrow 5CaCO_3 + 5H_2O \quad (b)$$

Beside PLA-HA, recent studies showed the benefits upon the application of other bioplastic sources to be used as additives for self-healing mortar, such as alkanoate derivatives (AKD) [38]. The production costs of these bioplastics are several times higher than the petro-chemical based plastics. According to Stabnikov et al. [39] a potential strategy to minimize the cost of production associated with these bioplastics to be incorporated into the self-healing application of concrete is the use of inexpensive raw materials from municipal solid waste, liquid waste from municipal wastewater treatment plants, food waste or agricultural waste for the extraction of AKD healing agents. Vermeer et al. [40] investigated the influence of the AKD healing agents (2.6% by weight of cement), comprising of 97.6% alkanoate, 0.39% spores and 0.019% nutrients in the self-healing performance of the mortar and reported an improvement in the self-healing efficiency for the first time. Similarly, Rossi et al. [37] studied the influence of AKD healing agents at 2.6% dosage on the recovery of mechanical properties and watertightness. These studies indicate that the addition of AKD healing agents considerably improve the self-healing performances of mortar specimens in comparison to control. This can be explained due to the production of carbon dioxide by the alkanoate derivate organic substrate which is a copolymer composed of hydroxybutyric acid ($CH_3CH(OH)CH_2CO_2H$) and hydroxypentanoic acid ($CH_3CH_2CHOHCH_2CO_2H$) monomers. These monomers can be utilized by bacteria and completely degraded to CO_2 under aerobic conditions, as described below.

$$CH_3CH(OH)CH_2CO_2H + 4.5O_2 \rightarrow 4CO_2 + 4H_2O \quad (c)$$

$$CH_3CH_2CHOHCH_2CO_2H + 6O_2 \rightarrow 5CO_2 + 5H_2O \quad (d)$$

Since recent studies showed the potential benefits of AKDs as HA for self-healing mortar, it is fundamental to assess the properties of this newly proposed system also with regard to varying dosages of HA that is added in the fresh mixture. Furthermore, assessing the self-healing capacity through various techniques as a function of healing time is truly relevant to better evaluate the actual benefits of the system with regard to the durability of the material. The encapsulation of the AKD healing agents were done by powder compression technologies that can mimic the characteristics of the HA additive [41]. To assess the effect of these

bioplastic healing agents on the mortar specimens, quantification and characterization of the self-healing performance were conducted. The quantification of the self-healing efficiency was studied by visual observations of crack healing through stereomicroscope, recovery of watertightness by rapid water permeability test and quantification of the calcium carbonate precipitates by TGA. For the first time, the characterization of the precipitated calcium carbonate by the bioplastic healing agents were investigated by TGA and XRD. Furthermore, a comparative assessment of the self-healing ratios between various micro-scale techniques and correlation-variability studies of the crack width and water flow were performed by statistical analysis.

2. Materials and methods

2.1. Bioplastic healing agents

The PLA-HA were supplied by Basilisk B.V. (Delft, the Netherlands), composed of bacterial spores of *Bacillus cohnii*-related strains (0.1–2% by weight of the total PLA-HA), organic and inorganic nutrient salts (10.5–43%) and PLA (50–80%). The size of the PLA-HA was in the range of 0.5 to 1 mm with a density of 1200 kg/m^3.

The AKD-HA were composed of spores derived from *Bacillus Cohnii*, nutrients (yeast extract), and an organic carbon substrate (alkanoate copolymer) extracted from wastewater streams as mentioned in [40]. The 40 g (97.6% by weight of the total HA) of alkanoate copolymer were mixed with 0.01 g of bacterial spores 'S' (0.04%) and 0.81 g of yeast extract 'YE' (2%). The obtained mixture was roller compacted to thin sheets by applying heat for 30 s at 100 ± 10 °C, then grinding the sheets into powders that were sieved to obtain a sand size (0.5–1 mm). Besides the following procedure, a freeze-drying method was adopted to eliminate the agglomeration of the grounded particles. The preparation (encapsulation) of the AKD-HA was displayed in Fig. 1.

2.2. Preparation of mortar specimens

The specimens were prepared by using cylindrical plastic moulds of 60 mm long and with a diameter of 33.5 mm. Five types of mixtures were investigated for this study. These were - control mixture (CTRL) without healing agents, mixture with calcium lactate derivatives of 2.6% (PLA 2.6) and 5% (PLA 5.0) dosage by weight of cement and mixture with alkanoate-based derivatives of 2.6% (AKD 2.6) and 5% (AKD 5.0) dosage in the mortar mixture. The mixture contained ordinary Portland cement (CEM I 42.5N, ENCI, The Netherlands), varying sand fractions ranging from 0.125 mm to 2 mm, water, and healing agent. The detailed mix design is in accordance with EN-196-1 listed in Table 1. For evaluation of the self-healing efficiency of the mortar mixtures, twelve cylindrical specimens were cast per mixture. All specimens after casting were sealed with polyethylene cover at the opening of the air-tight plastic container moulds and were kept for curing in a room with standard temperature (20–23 °C) and greater than 95% RH for 28 days.

2.3. Experimental procedure

In this study, the self-healing capacity and the precipitation of calcium carbonate of the five different mortar mixtures were investigated through different experimental techniques. The experimental procedure for each series consisted of 12 cylinders cast from the mortar mixture (2–3 samples casted may be neglected based on poor crack creation). After 28 days of curing, the crack induction was introduced as a single stable crack ranging from 0.04 to 0.8 mm. To prevent the dislodge of the specimens, an adhesive tape was attached around the curved surface of the cylinder. The crack in the specimens was visualized by stereomicroscope, followed by rapid water permeability test of the cracked specimens. From each series of 12 specimens, 1 random specimen was chosen for TGA and XRD analysis. The precipitated crystals at the crack mouth of these specimens were quantified using TGA and characterized using XRD. Two healing durations for crack healing were implemented – 28 and 56 days of healing in water (full immersion) accompanied by a similar self-healing assessment process. Fig. 2 depicts the experimental procedure for each series.

2.4. Crack calibration

After the curing period, the cracks were introduced in the specimens by tensile cracking. Initially, two (2 mm wide and 3 mm deep) notches were sawn at diametrically opposite ends of a cylinder's base layer. These notches ran down along the entire longitu-

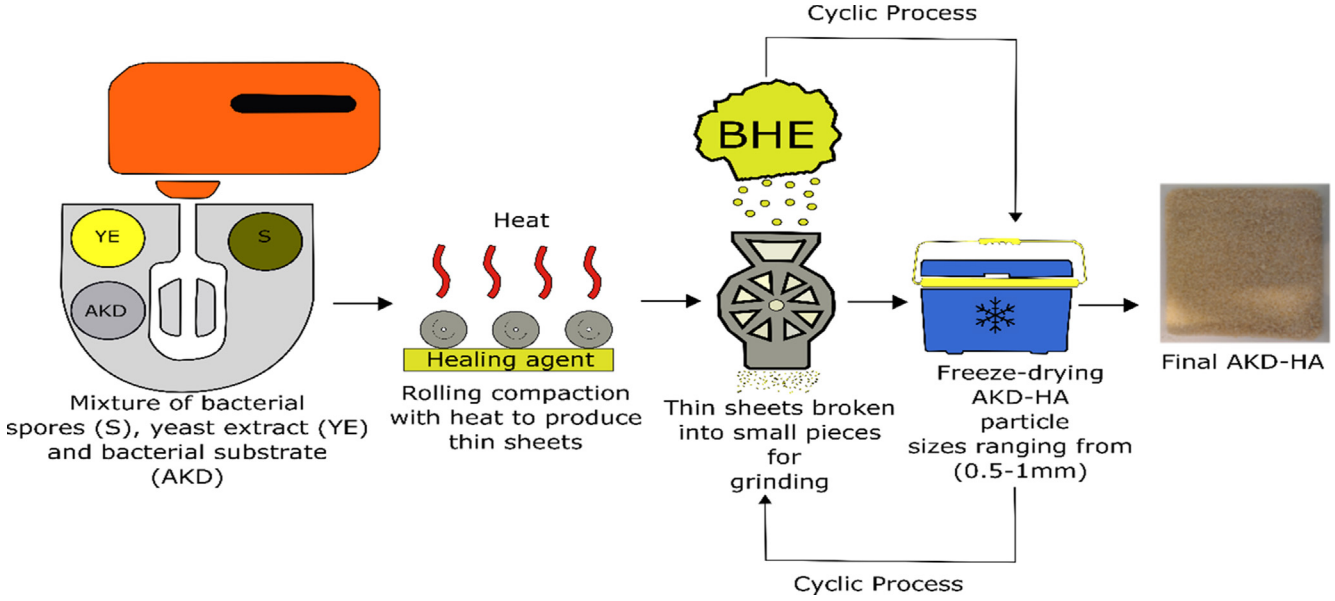

Fig. 1. Preparation of AKD-HA particles. "BHE" indicates the healing agent sheets comprising of S, YE and AKD.

Table 1
Mixing proportions of mortar specimens.

Mixture	Constituent	Amount (kg/m^3)	
CTRL; PLA 2.6; PLA 5.0; AKD 2.6; AKD 5.0	Cement	500	
	Water	250	
	Sand		
	fraction	495	
	(mm)	510	
	1–2	315	
	0.5–1	180	
	0.25–0.50	0.5	
	0.125–0.25		
	w/c ratio		
PLA 2.6; AKD 2.6; PLA 5.0; AKD 5.0	Healing agent	Dosage-2.6%	Dosage-5.0%
	PLA/AKD	14	26

dinal stretch of the cylinder's curved surface. Steel rods were placed along the created notches and adhered to the surface with adhesive tape to support the symmetrical notches during tensile cracking. Compressive loading speed of 0.01 ms-1 was applied along the placed steel rods by using Instron 8872 servo hydraulic hand press machine. The load was applied until the cylinders diametrically split along the created notches. Crack widths ranging between 0.04 and 0.8 mm were obtained. Finally, Perspex spacers of 2.4 mm wide were placed between the notches to fill the gaps created by the notches. Besides, the adhesive tape served to hold the two halves of the specimen together. This was done to provide a suitable crack width without dislodging the pieces into two halves. Fig. 3 depicts the crack creation procedure for the upcoming experiments.

2.5. Crack evaluation by stereomicroscope

The cracks at the specimen ends were evaluated through stereomicroscopic observations. The crack images were taken before and after healing for 28 and 56 days in tap water (full- immersion) for each specimen. Quantifying the crack in the specimen was achieved by labeling 10 positions along the crack length perpendicular to the crack path. These markings were equally spaced from each other along the crack length. The estimated crack width was obtained by averaging these marked values for each specimen. The estimated crack width from the top and the bottom face were used to determine the effective crack width of the specimen using Equation (1) [42].

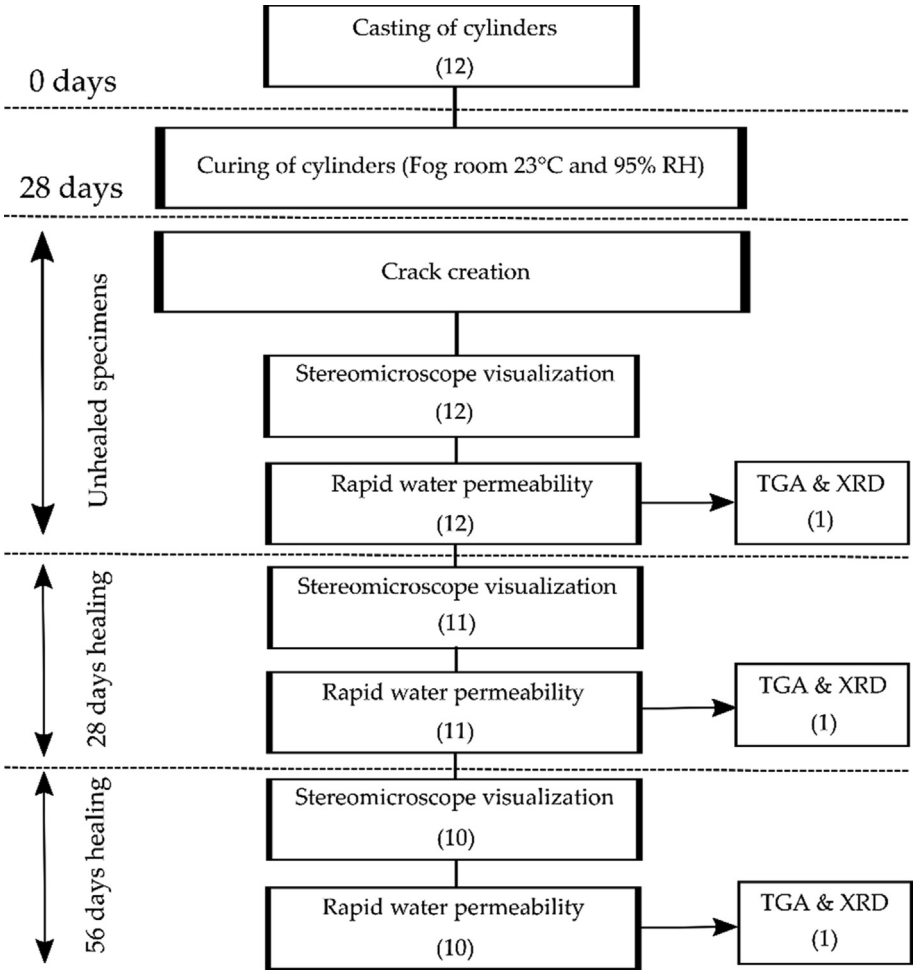

Fig. 2. Schematic representation of the experimental procedure (number of specimens for each series).

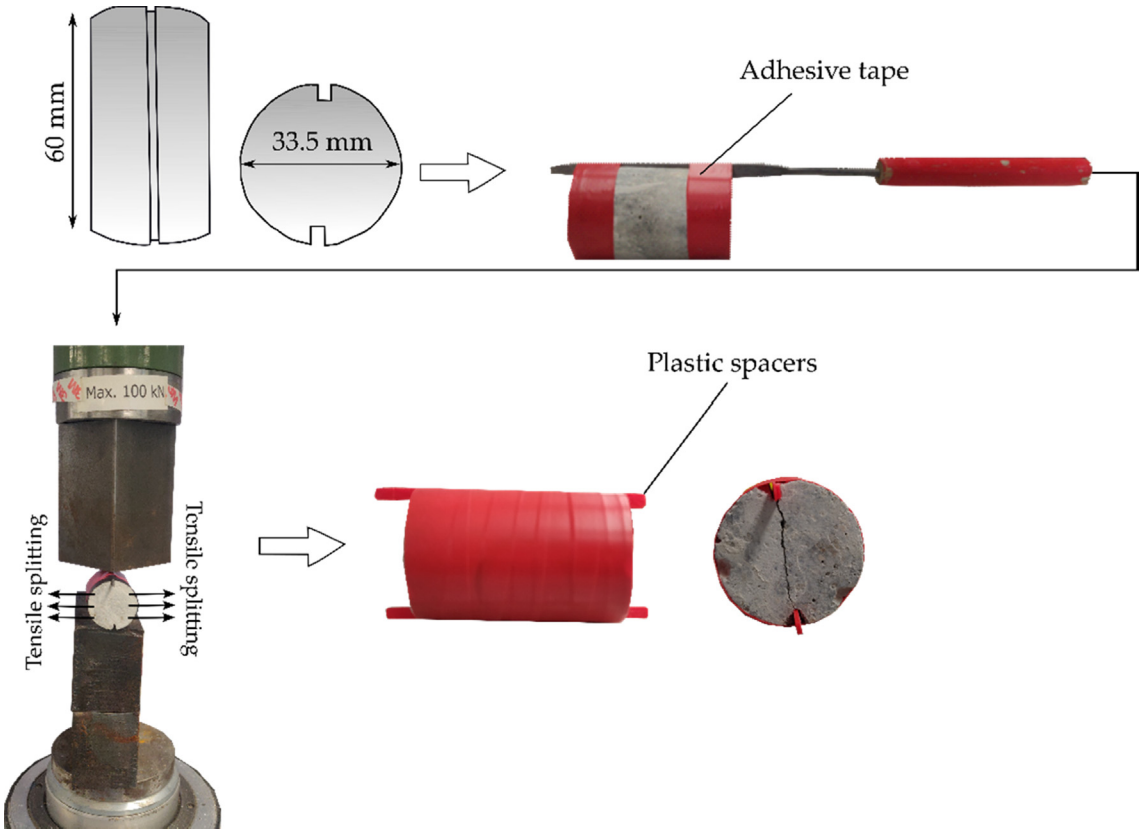

Fig. 3. Crack creation for the experimental procedure.

$$\text{Effective crack width}(Weff) = \frac{\sqrt[3]{2(TF \times BF)^2}}{TF + BF}(\text{mm}) \quad (1)$$

where *TF* and *BF* are the top face and bottom face in mm, respectively. To quantify the crack healing capacity of the specimens, the crack healing percentage was obtained using Equation (2).

$$\text{Crack healing percentage } (\%) = [(C_0 - C_t)/C_0] \times 100 \quad (2)$$

where C_0 is the initial effective crack width before healing in mm, and C_t is the final effective crack width after 28/56 days of healing in mm.

2.6. Rapid water permeability test

The self-healing efficiency was initially investigated through stereomicroscopic images. Despite stereomicroscopic observations, the results should be combined with a crack permeability test to relate functional property (water permeability) with visual observations. The permeability of the test specimens was determined by monitoring the weight of the leaked water through the cracks at a constant hydraulic water head of 0.1 bar. The test set-up as proposed by Palin et al. [43] was adopted for water permeability measurements. The coefficient of the water permeability (k) was obtained using Equation (3).

$$\text{Water permeabilitycoefficient}(k) = c \times Q(t)/t(\text{g/sec}) \quad (3)$$

where $Q(t)$ is the weight of water transported through surface of specimen in g as a function of time, t is the duration of the test conducted for the water to flow through the cracks of the specimen in sec, and c is the coefficient depending on the thickness of the specimen, hydraulic head and nominal crack length. Here c is assumed as 1. The recovery of water tightness (RWT) due to the self-healing effect was calculated by using Equation (4).

$$\text{RWT } (\%) = [(q_0 - q_t)/q_0] \times 100 \quad (4)$$

where q_0 is the initial water flowing through the cracks before healing period and q_t is the final water flowing through the cracks after a healing period of 28/56 days, measured in cm^3/sec.

2.7. Crack width and water flow

A crack flow model was proposed in which the water permeability (k) as a function of effective crack width (W_{eff}) were depicted for the observed values (experimental data) and the predicted values of the model. The predicted values were calculated using Poiseuille's Law, as stated in Equation (5).

$$\text{Water permeability}(q) = \xi \times \Delta P \times l \times {W_{eff}}^3/12 \times \eta \times d(\text{g/sec}) \quad (5)$$

where ΔP is the differential water pressure between crack inlet and outlet in Nm^{-2}, l is the nominal crack length across the face of the cylindrical specimen in m, w is the crack width in m, d is the crack depth which is the distance between the two faces of the cylindrical specimen in m, and η is the dynamic viscosity of the water in Ns m^{-2}. The water flowing through these cracks have a roughness and tortuosity that reduces the flow of water through these cracks. This effect is accounted by the reduction factor ξ.

2.8. Investigation of precipitated crystals at the crack mouth

The investigation of the self-healing product i.e. the precipitates sealing the cracks ($CaCO_3$ crystals) were subjected to XRD analysis (Philips PW 1830-XRD, Netherlands). The sample preparation for the XRD analysis was done by initially scrapping out the precipitates in the crack by using a scalpel. These scrapped materials were quenched using methanol inside a desiccator to provide longer

storage, thus promoting the hydration stoppage by solvent exchange. After the hydration stoppage, the material was ground by hand in an agate mortar-pestle, and methanol was added to prevent agglomeration and promote the fineness of the particle with sizes around 10–30 μm. Besides, sample spinning was done to ensure more particles to diffract at a given angle and reduce the error in the measured intensities. The powdered sample was placed in the aluminum holder by front loading and was subjected to a CuKα radiation with tube settings at 45 kV and 40 mA. The samples were scanned in the 2θrange of 5–70° with a step size of 0.030° 2θ and at a rate of 3 sec per step for data collection.

TGA was used as a complimentary technique to XRD for characterization of calcium carbonate precipitated crystals. Moreover, TGA was implemented for quantification of the calcium carbonate crystals. TGA and differential thermogravimetric (DTG) scan were performed simultaneously using a NETSCH STA 449 F3 Jupiter machine with a temperature interval of 40 °C–900 °C under a argon atmosphere. The heating rate was 10 °C/min. The sample preparation for TGA involved grinding the precipitated product ($CaCO_3$) by hand mortar-pestle under argon gas atmosphere, followed by pretreatment of the sample using a three-step procedure. This involved using isopropanol (exchange of pore water by isopropanol), followed by the removal of isopropanol by diethyl ether and short drying at 40 °C to evaporate any remaining diethyl ether. The sample was then kept for shorter durations in a closed container under light vacuum conditions. The weight of the scrapped sample varied between 16 and 52 mg. $CaCO_3$ decomposes above 600 °C to calcium oxide (CaO) and carbon dioxide (CO_2). The amount of $CaCO_3$ present in the cracks can be obtained by determining the weight loss of $CaCO_3$ from the TGA curve and using Equation (6).

$$\text{Amount of } CaCO_3 \text{in the crack mouth } (M_{CaCO3}) = W_L \times mCaCO_3/mCO_2(\text{mg}) \quad (6)$$

where W_L is the weight loss of $CaCO_3$ in mg, $mCaCO_3$ and mCO_2 are the molecular masses corresponding to 100 g/mol and 44 g/mol, respectively. To quantify the self-healing efficiency in terms of mass % of $CaCO_3$ precipitates formed before and after the healing period, Equation (7) was adopted.

$$\text{Self - healing efficiency } (\%) = [(M\%_{CaCO3(56)} - M\%_{CaCO3(28)})/M\%_{CaCO3(28)}]100 \quad (7)$$

where $M\%_{CaCO3(28)}$ and $M\%_{CaCO3(56)}$ are the mass % of the $CaCO_3$ precipitates formed at 28 and 56 days of healing, respectively.

3. Results

In the following sections, the results of this study will be shown and elaborated. Section 3.1 presents the analysis of the crack width at different healing periods followed by Section 3.2 which elaborates the flow of the water through these cracks and the recovery of water tightness of the specimen. Section 3.3 elucidates the parameters influencing the water permeability of the cracked specimens and the variability in the water flow and crack width. In the end, Section 3.4 provides the details on characterization of the precipitated products by the healing agents.

3.1. Stereomicroscope observations

3.1.1. Crack healing capacity at the TF and BF

Fig. 4 illustrates the crack width obtained at the TF and the BF of the specimens for each series as function of the healing period. From Fig. 4, initial reference crack widths were chosen to compare

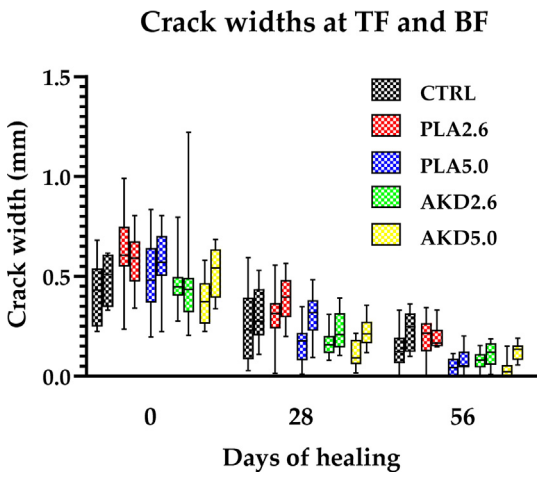

Fig. 4. Crack widths at the TF and BF as a function of increasing healing period. The left bar indicates the TF, and the right bar indicates the BF for each mortar series.

the crack closure efficiency between different series at different healing periods. At 28 days of healing, two reference initial crack width ranges of TF were chosen. In the first case, ranges from 0.19 mm to 0.40 mm were chosen in which CTRL, PLA2.6, PLA5.0, AKD2.6 and AKD5.0 series comprised of four, one, three, four and six specimens, respectively. In the second case, ranges from 0.4 mm to 0.6 mm were adopted. The number of specimens in these range were four, four, six, seven and four for CTRL, PLA2.6, PLA5.0, AKD2.6 and AKD5.0, respectively. In the case of 56 days of healing, same reference initial crack width ranges of TF were chosen with same number of samples. In the BF, the reference initial crack width ranges of 0.33 mm to 0.62 mm were chosen in which CTRL, PLA2.6, PLA5.0, AKD2.6 and AKD5.0 had nine, six, eight, seven, and seven respectively for 28 days of healing. At 56 days of healing, same reference initial crack width range was chosen but the number of samples varied for PLA5.0 which was seven in this case. Table 2 highlights the number of specimens for each reference crack widths at TF and BF.

Table 3 enlists the average self-healing capacity at the TF and BF for each mortar series. According to the results obtained, the average self-healing performance increased at higher healing durations for all the mortar series. CTRL series reported an increase in average self-healing ratio from 39% and 34% at TF and BF, respectively, for 28 days of healing to 68% and 53% at TF and BF respectively for 56 days of healing. Meanwhile, the bacteria containing series, especially PLA5.0 and AKD5.0 reported the maximum average self-healing efficiency at 28 and 56 days of healing. For PLA5.0, the self-healing efficiency observed at 28 days of healing were 68% and 49% for TF and BF respectively whereas at 56 days of healing, these self-healing efficiencies reached 92% and 87% for TF and BF, respectively. Similarly, for AKD5.0, the self-healing efficiency increased from 73% to 92% for the TF and 57% to 76% for the BF,

Table 2
Number of specimens for each reference crack widths of TF and BF.

Series	Number of specimens		
	TF	BF	
Ref. crack widths	0.19 mm–0.40 mm	0.4 mm–0.6 mm	0.33 mm–0.62 mm
CTRL	4	4	9
PLA2.6	1	4	6
PLA5.0	3	6	8
AKD2.6	4	7	7
AKD5.0	6	4	7

Number of specimens at each healing duration were same except for BF at 56 days of healing, PLA5.0 had 7 specimens.

Table 3
Average self-healing capacity of TF and BF at different healing periods for each mortar series.

Series	Healing Duration (days)			
	28		56	
	TF	BF	TF	BF
CTRL	39%	34%	68%	53%
PLA2.6	53%	32%	69%	67%
PLA5.0	68%	49%	92%	87%
AKD2.6	63%	50%	84%	76%
AKD5.0	73%	57%	92%	76%

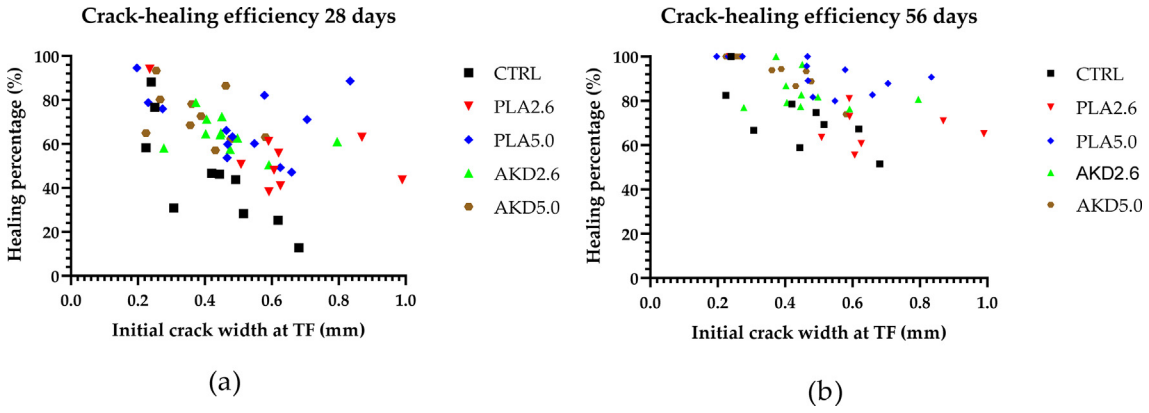

Fig. 5. Crack healing percentage against initial crack widths at TF for different healing periods: (a) 28 days and (b) 56 days.

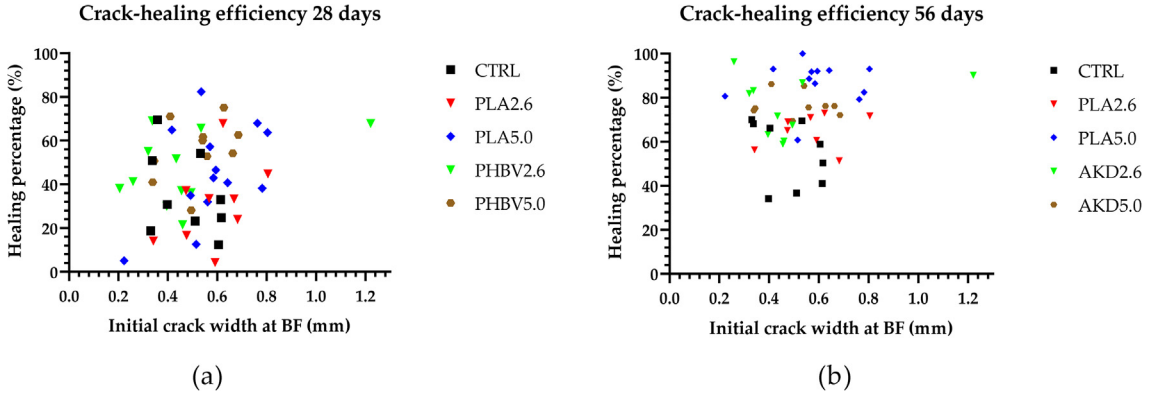

Fig. 6. Crack healing percentage against initial crack widths at BF for different healing periods: (a) 28 days and (b) 56 days.

as the healing period increased. Moreover, from the obtained values of self-healing efficiency at TF and BF, the self-healing at the BF was lower in comparison to the TF.

To distinguish the self-healing performance at individual crack widths for TF and BF obtained using image analysis application-ImageJ, self-healing efficiency was plotted against the initial crack widths of the TF and BF for different healing periods, as shown in Fig. 5 and Fig. 6, respectively.

According to Fig. 5 (a), for crack widths less than 0.4 mm, PLA5.0, PLA2.6, AKD5.0, AKD2.6 and CTRL reported the best self-healing performance of 94.6%, 94%, 93.4%, 78% and 88% for crack widths 0.19 mm, 0.23 mm, 0.25 mm, 0.36 mm and 0.23 mm respectively. At crack widths greater than 0.4 mm, PLA5.0 and PLA2.6 had higher self-healing efficiencies of 88.5% and 63.1% for crack widths 0.83 mm and 0.86 mm, respectively. However, for crack widths ranging between 0.4 and 0.6 mm, AKD5.0 had achieved the highest self-healing efficiency of 86% at a crack width of 0.46 mm in comparison to the other bacterial containing series and CTRL specimens. Overall, the self-healing performance of PLA5.0 at 28 days of healing was comparatively higher for most of the specimens in comparison to the other mortar series. In Fig. 5 (b), for crack widths less than 0.4 mm, a complete self-healing efficiency was achieved for CTRL, PLA2.6 and PLA5.0 at crack widths of 0.23 mm whereas for AKD2.6 and AKD5.0, 100% self-healing performance was reported at crack widths of 0.37 mm and 0.25 mm, respectively. However, PLA5.0 also achieved a complete crack closure for crack widths 0.19 mm and 0.27 mm whereas AKD5.0 also achieved a 100% self-healing performance at 0.22 mm and 0.26 mm. For crack widths greater than 0.4 mm, a complete crack closure was only observed for PLA5.0 at a crack width of 0.46 mm. Overall, for PLA and AKD at 5% dosage, a 100% self-healing efficiency was achieved for four different crack widths and three different crack widths, respectively. Meanwhile for CTRL and PLA/AKD at 2% dosage achieved a complete crack closure for only one time.

According to Fig. 6 (a), for crack widths less than 0.7 mm, PLA5.0, AKD5.0, AKD2.6, CTRL and PLA2.6 reported the best self-healing performance of 82.3%, 75.1%, 69%, 69.5% and 67.9% for

crack widths 0.53 mm, 0.62 mm, 0.33 mm, 0.35 mm and 0.62 mm respectively. For crack widths greater than 0.7 mm, PLA5.0 had a higher self-healing performance of 67.9% at a crack width of 0.76 mm in comparison to PLA2.6 and AKD2.6 which reported a high self-healing performance of 44% and 67.8% at crack widths of 0.8 mm and 1.2 mm respectively. Overall, the highest self-healing performances of PLA5.0 and AKD5.0 were achieved for different crack widths in comparison to other mortar series. In Fig. 6 (b), for crack widths less than 0.7 mm, only PLA5.0 achieved a complete crack closure at a crack width of 0.53 mm whereas for crack widths greater than 0.7 mm, PLA5.0 and AKD2.6 reported a self-healing efficiency of 93% and 90% at a crack width of 0.8 mm and 1.2 mm, respectively. Hence the self-healing performance improved for both the TF and BF as the healing period increased.

3.1.2. Crack healing capacity of the obtained effective crack width

Fig. 7 illustrates the effective crack width obtained for each mortar series as a function of the healing period. These effective crack widths were calculated using Equation (1). The initial effective crack widths of the CTRL series ranged from 0.21 to 0.61 mm. PLA2.6 and PLA5.0 had crack widths ranging from 0.36 to 0.7 mm and 0.30 to 0.8 mm, respectively, while AKD2.6 and AKD5.0 had crack widths ranging from 0.3 to 0.63 mm and 0.34 to 0.51 mm, respectively. At 28 days of healing, a diminishing trend in the effective crack widths were observed. For CTRL series the effective crack widths were in the range of 0.06 to 0.47 mm. In the case of PLA2.6, the effective crack widths were in the range of 0.04 to 0.43 mm. PLA5.0 had effective crack widths in the range of 0.09 to 0.39 mm. For AKD2.6 the crack widths were in the range of 0.12 to 0.22 mm whereas AKD5.0 had crack widths in the range of 0.05 to 0.24 mm.

This diminishing trend was further enhanced at 56 days of healing. In the CTRL series, the crack widths reduced to the range of 0 to 0.32 mm. Similarly, for PLA2.6, the cracks widths were in the range of 0 to 0.22 mm. In PLA5.0, the crack widths were in the range of 0 to 0.14 mm. AKD2.6 had crack widths in the range of 0 to 0.12 mm whereas AKD5.0 had crack widths in the range of 0 to 0.08 mm.

Table 4 enlists the average self-healing capacity of effective crack widths for each mortar series. According to the results obtained, the self-healing performance at the effective crack widths improved with the increasing healing period for all the mortar series. In the CTRL series, the average self-healing efficiency increased from 30% at 28 days of healing to 61% at 56 days of healing. In the case of bacteria containing series especially PLA and AKD at 5% dosage, maximum self-healing efficiency of 60% and 69% was reported for PLA5.0 and AKD5.0 at 28 days of healing respectively, which further increased to 92% and 90% at 56 days of healing.

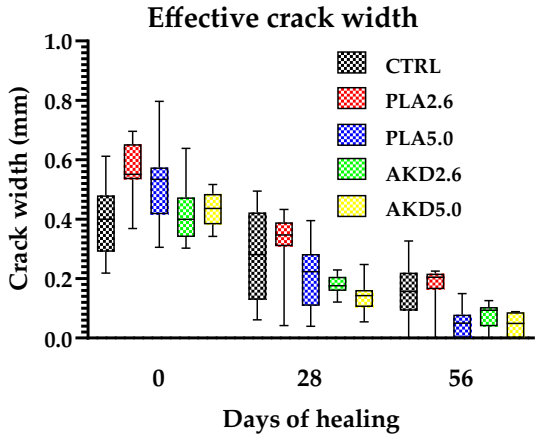

Fig. 7. Effective crack width as a function of increasing healing period.

Table 4
Average self-healing capacity of effective crack width at different healing periods for each mortar series.

Series	Healing Duration (days)	
	28	56
CTRL	30%	61%
PLA2.6	44%	70%
PLA5.0	60%	92%
AKD2.6	56%	82%
AKD5.0	69%	90%

Hence an improved self-healing performance was more significant for PLA5.0 and AKD5.0.

To distinguish the self-healing performance at individual effective crack widths, self-healing efficiency was plotted against the initial effective crack widths for different healing periods, as shown in Fig. 8. For initial effective reference crack widths ranging between 0.28 and 0.4 mm, highest self-healing performance at 28 days was achieved for CTRL, PLA2.6, PLA5.0, AKD2.6 and AKD5.0 corresponding to self-healing efficiency of 78%, 88%, 89%, 67% and 86% at crack widths of 0.28 mm, 0.36 mm, 0.36 mm, 0.36 mm and 0.39 mm, respectively. At 56 days of healing, best self-healing efficiency was reported in which CTRL specimens achieved a 100% self-healing for effective initial crack width of 0.28 mm. In addition, for reference effective cracks ranging from 0.36 to 0.4 mm, all series-containing healing agents, achieved 100% crack closure. In contrast, CTRL specimens exhibited a self-healing ratio of 72% and 77% for an effective crack width of 0.39 and 0.33 mm, respectively. These findings suggest that the occurrence of complete crack closure is more frequent for small effective crack widths. Moreover, bacteria containing series especially PLA5.0 and AKD5.0 had achieved a complete crack closure three times in comparison to other mortar series which achieved only one time. Fig. 9 shows the stereomicroscopic observations of the crack healing capacity for cracks in the range of 0.36 to 0.4 mm at 56 days healing period.

The stereomicroscopic observations reveal that except for CTRL series, no indication of cracks on the cracked specimens for PLA and AKD series were reported at 56 days of healing. Thus, a complete crack closure could be observed for PLA and AKD series at 56 days healing period for cracks in the range of 0.36 to 0.4 mm.

Series containing healing agents displayed much higher self-healing ratios for initial reference effective crack widths in the range of 0.4 mm to 0.8 mm. At initial effective crack width ranging between 0.4 and 0.5 mm, CTRL specimens displayed a maximum self-healing ratio of 72% for crack width of 0.40 mm compared to AKD2.6 which exhibited a maximum self-healing ratio of 90% for a crack width of 0.45 mm at 56 days of healing. At crack widths ranging between 0.5 and 0.6 mm, higher crack closure ratios of 50.45% and 100% were achieved at 28 and 56 healing days respectively, for PLA5.0 compared to CTRL, which showed just 37% and 69% at 28 and 56 healing days, respectively. Moreover, a complete crack closure for PLA5.0 was reported for two times for a crack width of 0.52 mm and 0.55 mm at 56 days of healing. Fig. 10 depicts the stereomicroscopic images for cracked specimens of CTRL and PLA5.0 at different healing periods.

The stereomicroscopic observations reveal that for PLA5.0 cracked specimens, crack healing could be observed especially at the TF and BF due to filling of precipitated products by the healing agents. However, for CTRL cracked specimens only TF indicated the filling of the crack mouth whereas for BF crack filling could not be observed. For crack widths ranging between 0.6 and 0.8 mm, a higher sealing efficiency was obtained for series containing healing agents. PLA2.6 obtained a self-healing ratio of 54% and 77% at 28 and 56 days of healing, respectively for initial effective crack width of 0.79 mm. PLA5.0 achieved a self-healing ratio of 56% and 88% at 28 and 56 days of healing, respectively, for initial effective crack

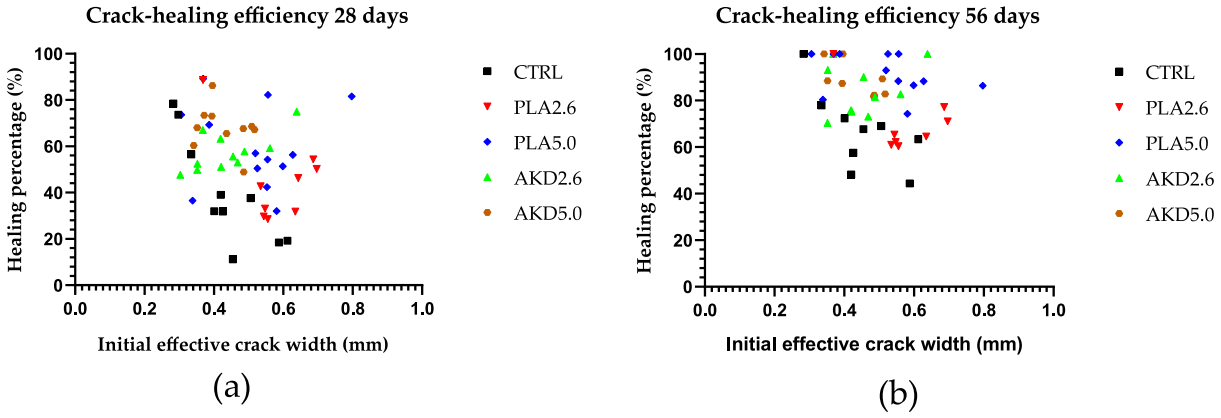

Fig. 8. Crack healing percentage against initial effective crack widths for different healing periods: (a) 28 days and (b) 56 days.

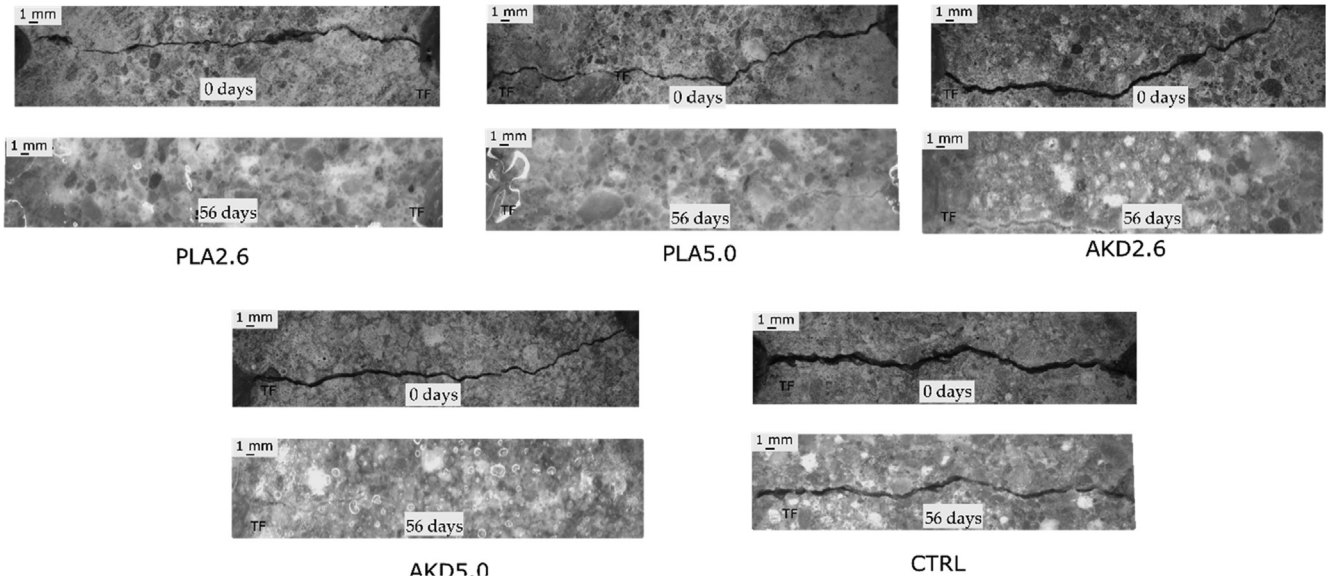

Fig. 9. Stereomicroscopic images of cracked specimens before and after 56 days of healing for initial effective crack widths of 0.39 mm, 0.36 mm, 0.36 mm, 0.36 mm and 0.34 mm for CTRL, PLA2.6, PLA5.0, AKD2.6 and AKD5.0 respectively. Top image of each mortar series corresponds to 0 days healing and bottom image corresponds to 56 days healing.

width of 0.62 mm. AKD2.6 achieved the best self-healing ratio of 75% and 100% at 28 and 56 days of healing, respectively, for 0.63 mm. On the contrary, at 28 and 56 days of recovery, CTRL specimens reached the lowest self-healing levels corresponding to 19% and 63%, respectively, for initial effective crack width of 0.61 mm at 28 and 56 days of healing, respectively.

3.2. Rapid water permeability test

3.2.1. Recovery of water tightness

To quantify the self-healing efficiency, recovery of water tightness was calculated using Equation (4). Fig. 11 depicts the range of self-healing efficiencies for different mortar series at different healing periods. The average self-healing efficiency of each mortar series was reported. AKD5.0 had the highest average self-healing ratios of 55.8% for initial effective crack widths (0.34–0.51 mm), followed by PLA5.0 (0.30–0.79 mm) with average self-healing ratio of 50%, AKD2.6 (0.30–0.63 mm) with average self-healing ratios of 47% and CTRL (0.21–0.61 mm) with an average self-healing ratio of 45% at 28 days of healing. Meanwhile, PLA2.6 reported the lowest average self-healing ratio of 38.5% at 28 days healing period. At 56 days of healing period, an average increase in the self-healing ratios were observed for all data series. However, this trend in the self-healing ratios were different compared to the obtained values at 28 days of healing. These values pertained to 71% for PLA5.0, followed by 65% for AKD5.0, 57% for AKD2.6 and 54% for CTRL specimens. PLA2.6 again recorded the lowest average self-healing ratio of 49% at 56 days of healing. Nevertheless, PLA5.0 and AKD5.0 recorded the best average performance at 56 days of healing compared to 28 days. To interpret these results further from Fig. 11, 80% of the samples in PLA5.0 had better self-healing efficiency for 56 days of healing compared to 50 percentiles of the CTRL specimens. However, as the PLA dosage decreased to 2.6 percent, only 30% of the samples had better self-healing efficiency than the 50 percentiles of the CTRL specimens. Furthermore, for AKD series, a similar trend was observed in the self-healing performance. At 2.6% dosage in AKD, 27% of the samples had higher self-healing efficiency compared to 50 percentile of CTRL specimens whereas at 5.0% dosage, 55% of the samples had a better self-healing efficiency in comparison to 50 percentile of CTRL specimens.

To distinguish the recovery of water tightness at individual crack widths, scatter plot was presented, as shown in Fig. 12.

For initial effective reference crack widths between 0.28 and 0.4 mm, CTRL series reported the highest recovery of water tightness of 97% for a crack width of 0.28 mm whereas PLA2.6, PLA5.0, AKD2.6 and AKD5.0 corresponded to 41%, 72%, 60% and

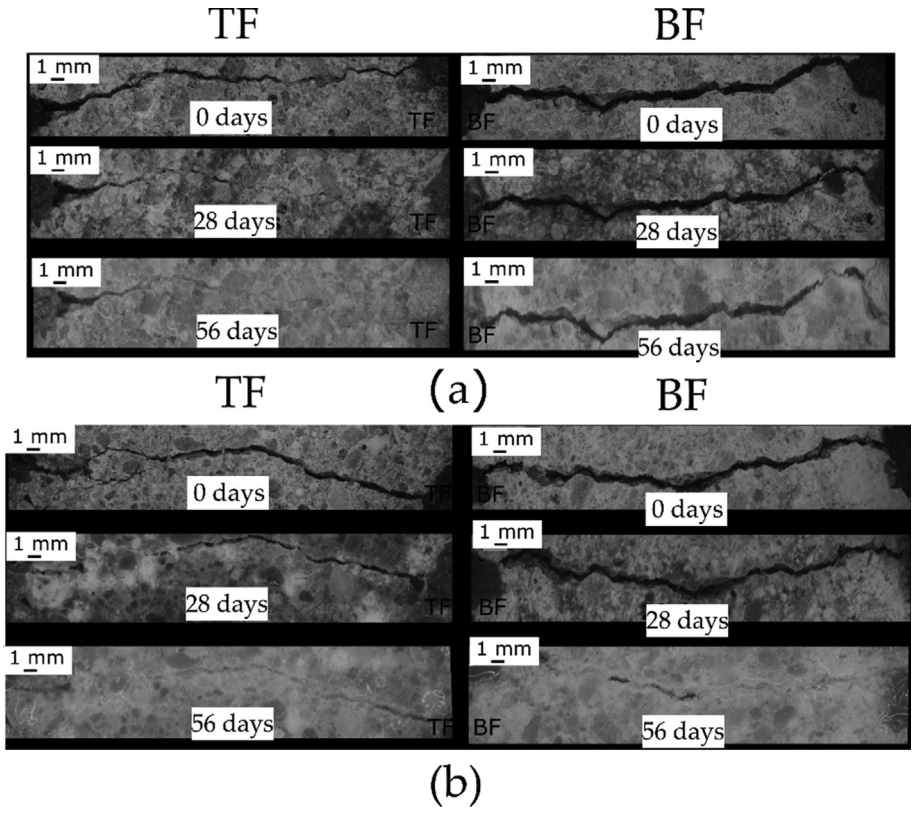

Fig. 10. Stereomicroscopic images of cracked specimens at 0, 28 and 56 days of healing for initial effective crack width of (a) 0.5 mm for CTRL and (b) 0.52 mm for PLA5.0.

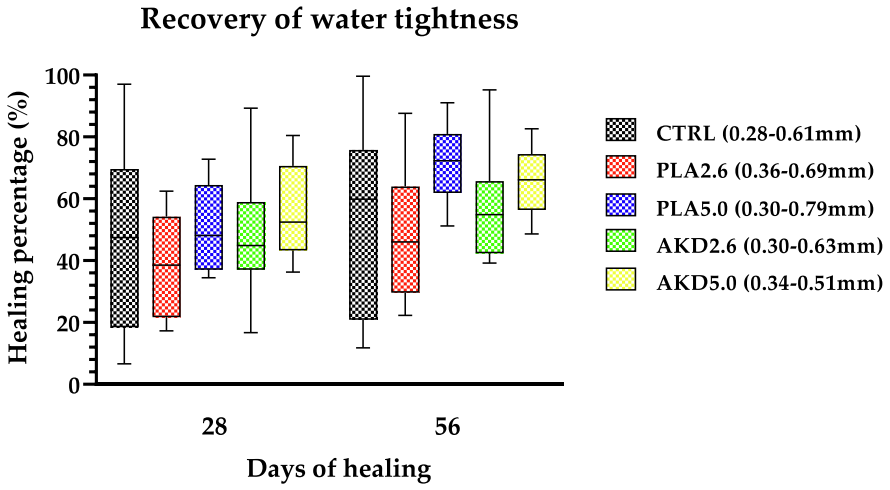

Fig. 11. Recovery of water tightness at different healing periods for each mortar series.

78% of recovery in water tightness for initial effective widths of 0.36 mm, 0.30 mm, 0.36 mm and 0.34 mm at 28 days of healing, respectively. Similarly, at 56 days of healing, CTRL series reported the best recovery of water tightness of 99% followed by PLA5.0 of 91%, 87% for PLA2.6, 82% for AKD5.0 and only 65% for AKD2.6. In the case of initial reference effective crack widths ranging between 0.5 and 0.56 mm, 80% recovery of water tightness was achieved for CTRL specimen for crack width of 0.50 mm in comparison to PLA2.6, PLA5.0, AKD2.6 and AKD5.0 which achieved a recovery of water tightness of 46% (0.54 mm), 48% (0.55 mm), 26% (0.56 mm) and 48% (0.51 mm) respectively at 28 days healing. During 56 days of healing, the recovery of water tightness of CTRL specimens increased to 82% whereas for PLA5.0, the self-healing efficiency increased to 72%, 68% for AKD5.0, 52% for AKD2.6 and 39% for PLA2.6. For initial effective crack widths ranging between 0.6 and 0.68 mm, AKD2.6 reported best recovery of water tightness of 89% and 95% at 28 and 56 days of healing respectively for effective crack width of 0.63 mm. In contrast, CTRL series recorded the lowest recovery of water tightness of 6.6% and 11% at 28 and 56 days of healing, respectively, for initial effective crack width of 0.61 mm.

3.3. Statistical analysis

3.3.1. Correlation between crack width and water flow

A relationship between water flow and effective crack width was proposed by Edvardsen et al. [44]. This relationship is presented in Equation (5) which states that the theoretical calculated

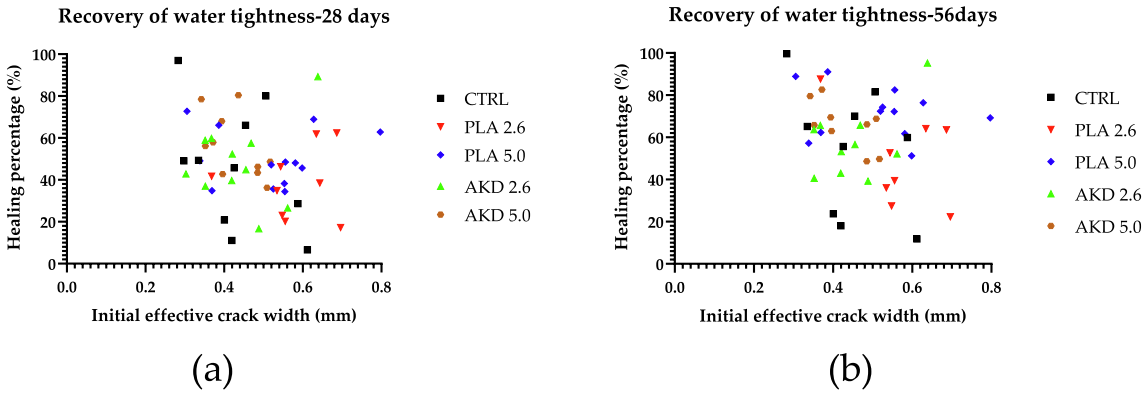

Fig. 12. Recovery of water tightness against initial effective crack widths for different healing periods: (a) 28 days and (b) 56 days.

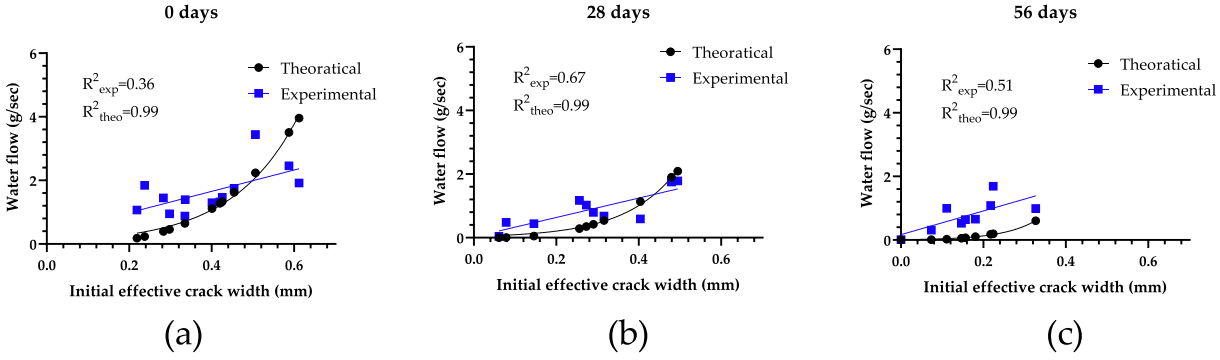

Fig. 13. Crack flow model for CTRL series at (a) 0 (b) 28 and (c) 56 days of healing.

water flow q is proportional to the third power of the effective crack width w in the specimen, i.e., as the effective crack width of the specimen increases, the waterflow increases dramatically. This theoretical crack flow model does not depend on the period of healing but is based on certain assumptions. These assumptions are parameter l is assumed to be equal to the crack length across the end face of the specimens (0.03 m) and parameter d is assumed to be equal to the crack depth between the end faces of the specimens (0.051 m). Small variations in the crack depth between the specimens due to casting, demoulding, and sawing are neglected. For all the data series at different healing durations, Δp was equal to 10,000 Pa (1 m of water column). Besides to account for the effects of the internal crack geometry for smaller crack widths, a reduction factor ξ was applied which was estimated as 0.031 and was obtained by rearranging the Equation (5) with substituted initial water permeability experimental values for q. Thus, a nonlinear function was obtained. Fig. 14 represents the crack flow model for the CTRL series at different healing periods.

According to Fig. 13, high R^2 constant values of 0.99 was accounted at different healing periods for the theoretical model due to the accounting of the internal crack geometry. Nevertheless, low R^2 values for the experimental data were reported. These variability in the result might not only arise from internal crack geometry but also from the variability due to the test method adopted. These include operator sensitivity, small changes in the environmental conditions, small changes in the water head, accuracy of the scale, small particles which detach from the crack wall and either block a certain part of the crack or were flushed out. This trend of low R^2 values were also identified in the bacteria containing series. Table 5 provides the correlation coefficients between the water flow and the effective crack width for the observed values in the bacteria containing specimens at 0, 28 and 56 days of healing.

3.3.2. Variability in crack width and water flow: coefficient of variation, standard deviation and mean

The variation in the water flow for initial effective crack width in the observed values of different mortar series can be explained by the concept of coefficient of variation (COV). The COV measures the relative event dispersion which is equal to the ratio between the standard deviation and the mean expressed by the Equation (8).

$$\mathrm{COV} = \frac{\sigma}{\mu} \tag{8}$$

where σ is the standard deviation and μ is the mean value of the observed data. According to Table 6 (a), the COV for the initial effective crack widths of the mortar series were in the range of 13–30%. These variations were quite large in comparison to the literature [45]. Moreover, the variation in the effective crack width increased as the healing period increased, as shown in Tables 6 (b-c). This indicates that the degree of self-healing in the mortar series is not equal for the same initial effective crack widths. In the case of quantification of crack healing capacity by stereomicroscope, PLA5.0 exhibited self-healing efficiency of 88% and 100% for the same initial effective crack width of 0.55 mm which verifies that the degree of self-healing may not be consistent for the same initial effective crack width.

Similarly, in the case of water flow through these cracks, a huge variation in the water flow was reported at higher healing periods. This can be partly explained by the high variations of the effective crack widths. Besides, the variations in the water flow in some cases were comparatively higher than their corresponding effective crack width variation. However, the variation in the crack width is not the sole factor for the recorded high variations in the water flow. This will be explained in more detail in the next sections.

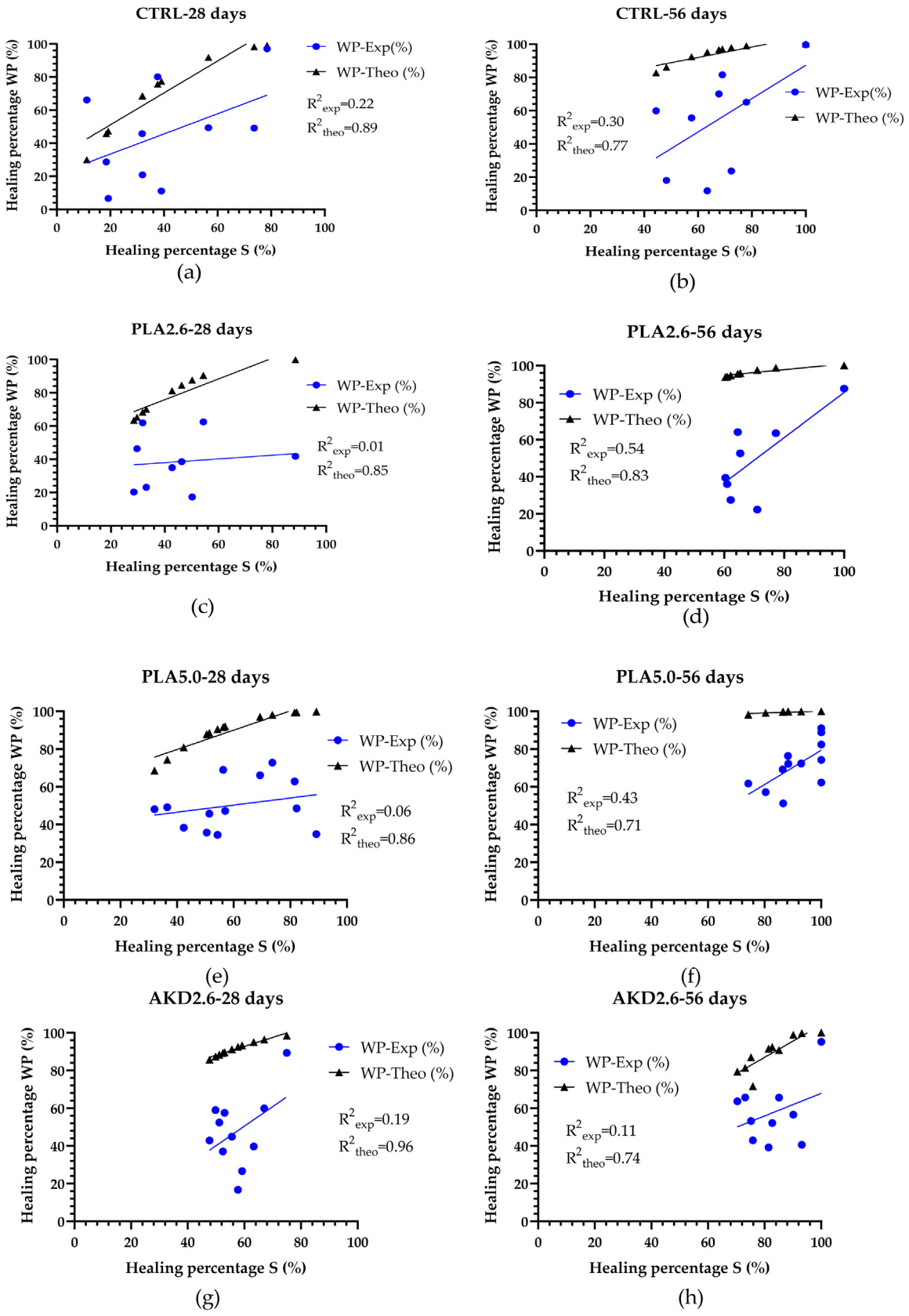

Fig. 14. Comparative assessment of self-healing efficiency by water permeability (WP) test and stereomicroscope (S). The *WP-Exp* stands for experimental data set and *WP-Theo* stands for theoretical data set for WP.

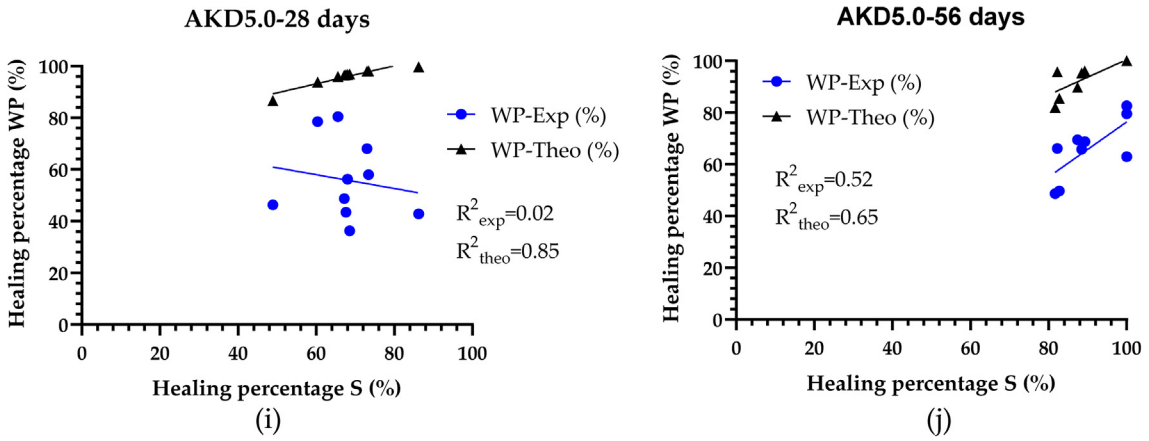

Fig. 14 (*continued*)

Table 5
Correlation coefficients (R^2) for observed values of crack flow model in bacterial containing series.

	Correlation (R^2)			
	PLA2.6	PLA5.0	AKD2.6	AKD5.0
0 days	0.16	0.22	0.46	0.25
28 days	0.33	0.54	0.36	0.44
56 days	0.56	0.45	0.10	0.81

Table 6a
Variation in effective crack width and water flow at 0 days healing.

Variation in effective crack width (W_{eff}) and water flow (q) at 0 days healing										
	CTRL		PLA2.6		PLA5.0		AKD2.6		AKD5.0	
	W_{eff} (mm)	q (g/s)	W_{eff} (mm)	q (g/s)	W_{eff} (mm)	q (g/s)	W_{eff} (mm)	q (g/s)	W_{eff} (mm)	q (g/s)
μ	0.39	1.63	0.57	1.71	0.51	1.14	0.41	0.95	0.43	0.96
σ	0.12	0.69	0.09	0.62	0.12	0.58	0.09	0.37	0.05	0.37
COV	0.30	0.42	0.16	0.36	0.23	0.50	0.24	0.39	0.13	0.38

Table 6b
Variation in effective crack width and water flow at 28 days healing.

Variation in crack width (W_{eff}) and water flow (q) at 28 days healing										
	CTRL		PLA2.6		PLA5.0		AKD2.6		AKD5.0	
	W_{eff} (mm)	q (g/s)	W_{eff} (mm)	q (g/s)	W_{eff}(mm)	q (g/s)	W_{eff} (mm)	q (g/s)	W_{eff} (mm)	q (g/s)
μ	0.27	0.87	0.32	1.07	0.20	0.59	0.18	0.57	0.13	0.43
σ	0.15	0.56	0.11	0.60	0.10	0.36	0.03	0.35	0.05	0.23
COV	0.54	0.64	0.34	0.56	0.50	0.61	0.18	0.61	0.37	0.54

Table 6c
Variation in effective crack width and water flow at 56 days healing.

Variation in crack width (W_{eff}) and water flow (q) at 56 days healing										
	CTRL		PLA2.6		PLA5.0		AKD2.6		AKD5.0	
	W_{eff} (mm)	q (g/s)	W_{eff} (mm)	q (g/s)	W_{eff} (mm)	q (g/s)	W_{eff} (mm)	q (g/s)	W_{eff} (mm)	q (g/s)
μ	0.15	0.76	0.17	0.96	0.05	0.37	0.07	0.46	0.04	0.34
σ	0.09	0.46	0.07	0.56	0.05	0.33	0.04	0.24	0.03	0.20
COV	0.59	0.60	0.42	0.58	1.00	0.90	0.55	0.53	0.84	0.58

3.3.3. Variability in water flow with same effective crack width: coefficient of variation, standard deviation and mean

According to the previous section, a huge variation in the water flow was observed for the mortar series besides its effective crack width variation. Nevertheless, variation in the crack width alone cannot account for the variation in the flow. In the case of identical crack widths, a significant variation in the water flow was still observed. Similar examples can be found in Table 7. These variations illustrate the importance of internal crack geometry. For equal effective crack width, the internal structure of the crack might differ causing variation in the water flow rate. Moreover, in accordance with Table 7, for larger effective equal crack widths,

Table 7
Variation in water flow with equal effective crack width.

Variation in water flow with equal effective crack width														
	CTRL-0		PLA2.6–0		AKD2.6–0		AKD5.0–0		PLA2.6–28		AKD2.6–28		PLA5.0–56	
	W_{eff} mm	q g/s	W_{eff} mm	q g/s	W_{eff} mm	q g/s	W_{eff} mm	q g/s	W_{eff} mm	q g/s	W_{eff} mm	q g/s	W_{eff} mm	q g/s
1	0.41	1.32	0.54	1.31	0.30	0.91	0.39	1.61	0.34	1.87	0.22	0.47	0.00	0.03
2	0.42	1.46	0.55	2.60	0.30	0.25	0.39	0.60	0.34	0.89	0.23	1.27	0.00	0.23
μ	0.42	1.39	0.55	1.96	0.30	0.58	0.39	1.11	0.34	1.38	0.22	0.87	0.00	0.13
σ	0.00	0.10	0.00	0.91	0.00	0.46	0.00	0.71	0.00	0.69	0.00	0.57	0.00	0.14
COV	0.00	0.07	0.00	0.46	0.00	0.79	0.00	0.64	0.00	0.49	0.02	0.65	0.00	1.00

Series Name-healing duration.

the variation in the water flow was comparatively lesser than the variation in the water flow for smaller effective equal crack widths. From Table 7, it was reported that for larger crack widths like 0.42 mm and 0.55 mm, the obtained COV in the water flow was lower corresponding to 0.07 and 0.46 respectively in comparison to smaller crack widths whose COV was greater than 0.46. This can be confirmed with the results obtained for the recovery of water tightness at 56 days of healing, PLA2.6 exhibited two different self-healing efficiency of 54% and 27% for the same initial effective crack width of 0.54 mm.

3.3.4. Comparative assessment of recovery of water tightness and crack healing capacity by regression analysis

The data from the self-healing quantification results revealed that the self-healing efficiency from the light microscopy and water permeability had quite a few variations for the same specimens of the mortar series. This is because in stereomicroscopic measurements, the crack healing capacity is calculated based on efficient self-healing of the crack width, while in the case of a water permeability test, the self-healing capacity is measured in terms of resistance to water flow due to self-healing of cracks. In the quantification of the crack healing capacity by stereomicroscope, the best self-healing efficiency of the bacteria containing series obtained were 100% for PLA5.0 and AKD5.0 at a crack width of 0.3 mm and 0.34 mm respectively for 56 days healing period. However, the best recovery of water tightness by rapid water permeability test corresponded to 91% and 82% for PLA5.0 and AKD5.0 respectively at 56 days of healing. This means that even though the effective width of the crack is 100% sealed, the resistance to water flow may not be 100%.

To understand the correlation between self-healing efficiencies by stereomicroscope and rapid water permeability test, regression analysis was conducted as shown in Fig. 14 (a-j). In this study, the theoretical and experimental values of the self-healing efficiencies from the permeability test were compared with the self-healing efficiency by stereomicroscope. In the experimental data, the trend indicated that the data points are spread out further from the trend (low R^2 values) line compared to the theoretical model. This implies that the prediction interval for the experimental case is broader compared to the theoretical counterpart. Thus, in the experimental data, precision of predicting the self-healing efficiency of the water permeability from the self-healing efficiency by stereomicroscope is quite low compared to the theoretical case. Hence when evaluating self-healing efficiency, the data obtained from a singular experimental technique might not provide the precise predictions of self-healing efficiencies for other experimental techniques. Moreover, most of the series except PLA2.6, PLA5.0 and AKD2.6 at 56 days of healing exhibited p-values higher than the significant level. This implies that there is insufficient evidence to conclude that a non-zero correlation exists between the self-healing efficiencies. Hence in this scenario, a change in the self-healing efficiency by stereomicroscope may not provide a corresponding accurate change in the self-healing efficiency for

Table 8
Variation in water flow with equal effective crack width.

Series	Crystallite size (μm)	
	$CaCO_3$	
Healing duration	28	56
CTRL	17.39	17.30
PLA2.6	20.12	26.83
PLA5.0	23.32	23.60
AKD2.6	21.78	23.40
AKD5.0	25.26	25.51

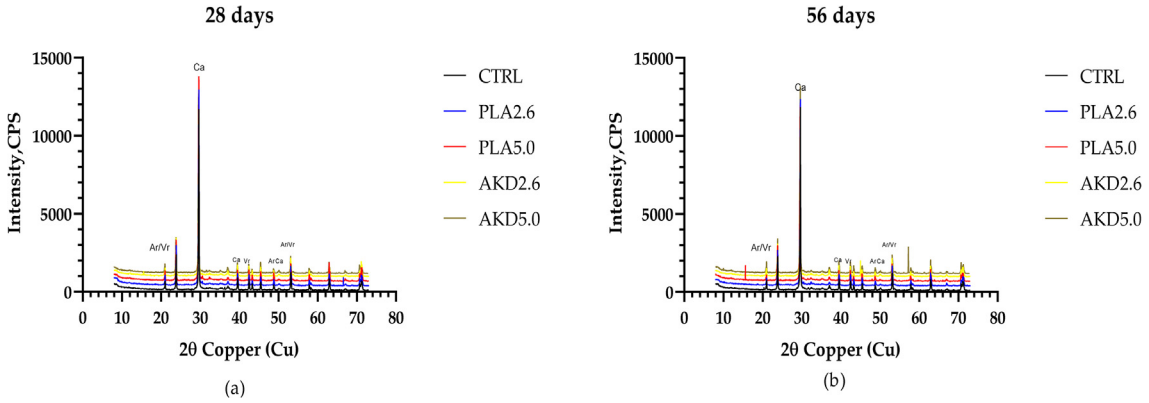

Fig. 15. XRD spectrum at (a) 28 and (b) 56 days of healing.

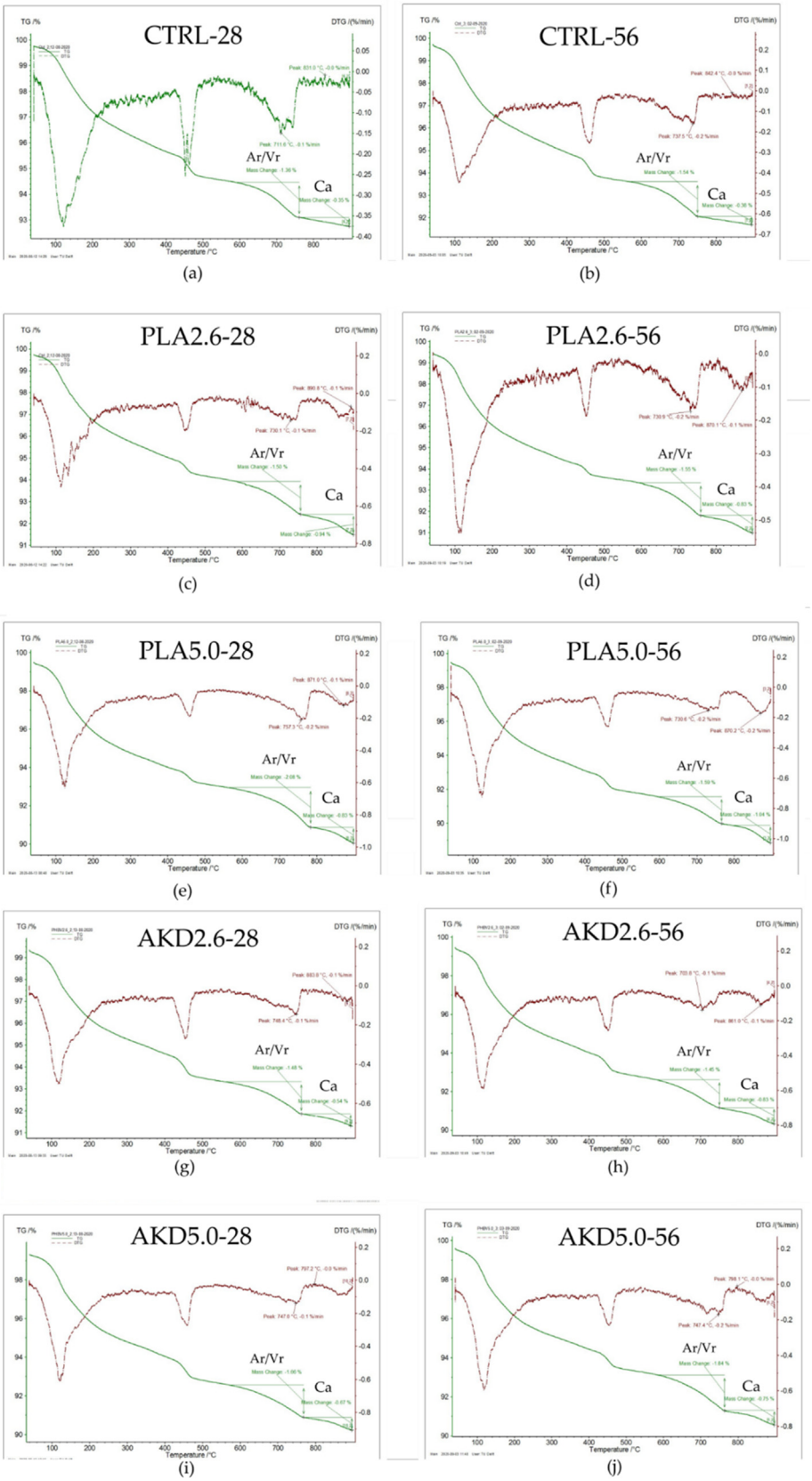

Fig. 16. TGA and DTG profiles for each mortar series at 28- and 56-days healing period. Ca represents the calcite peak and the weight loss and Ar/Vr represent the aragonite/vaterite peak and the weight loss.

the water permeability test since the parameters used for assessing the self-healing efficiency in both experimental techniques are quite different.

3.4. Characterization of precipitated crystals by healing agents at the crack mouth

3.4.1. X-ray diffraction analysis

The $CaCO_3$ precipitated in the vicinity of the cracks were identified by using X-ray diffraction analysis. According to Fig. 15 (a-b), the XRD patterns obtained for different series were almost similar at 28 and 56 days of healing. The presence of $CaCO_3$ in the cracks were confirmed by the XRD spectra indicating the presence of calcite, aragonite and vaterite at certain 2θ positions. At 28 days of healing, high intensity of calcite peak was observed at 2θ positions of 29.40°, followed by 39.45° and at 50°. These peak positions almost coincide with the pure calcite crystals from the XRD reference database. Besides, strong aragonite and vaterite peaks were also observed at 2θ positions of 20.86°, 42.4° and 53°. After 56 days of healing, similar peak patterns were observed, thus indicating the presence of calcite, aragonite and vaterite.

In this study, the maximum crystallite size of calcium carbonate obtained was differentiated for different mortar series having different self-healing mechanisms by using the Scherrer method [46]. The crystallite size D was obtained using Equation (9) from the XRD data.

$$D = \frac{k\lambda}{\beta_D \cos\theta} \tag{9}$$

where D is the particle size in nanometers, λ is the wavelength of the radiation (1.54056 Å for CuKα radiation), k is a constant equal to 0.94, β_D is the peak width at half-maximum intensity and θ is the peak position. Table 8 provides the details of maximum crystallite size of $CaCO_3$ found in the crack mouths at different healing periods for each mortar series.

According to Table 8, the maximum crystallite sizes obtained at 28 and 56 days of healing for the bacteria containing series were comparatively higher than the CTRL series. The sizes of the crystallites varied from 20 to 27 μm compared to CTRL series which had maximum crystallite sizes of 17.39 μm and 17.30 μm at 28 and 56 days of healing, respectively.

3.4.2. Thermogravimetric analysis

To investigate the production of $CaCO_3$ by the healing agents, TGA was adopted to quantify the self-healing action by the healing agents. Although the exact source of Ca^{2+} ions used by the bacteria during self-healing is unknown, it has been suggested that calcium hydroxide is likely to be the most significant source [47]. In addition, the availability of carbonate ions (CO_3^{2-}) at the vicinity of the cracks depends on the dissolved organic carbon concentration by the bacterial substrate (calcium lactate or alkanoate copolymer in this case). Therefore, these Ca^{2+} ions are attracted by the bacteria due to their negatively charged surface (CO_3^{-2}), indicating nucleation point around the cell walls thus precipitating calcium carbonate [48]. Bacteria produced $CaCO_3$ has three anhydrous crystalline forms; calcite, aragonite and vaterite. Among the three crystalline polymorphs, the thermodynamically most stable one is calcite and the least stable ones are aragonite and vaterite [49]. To confirm this proposition, TGA studies conducted by [50] reported that dissociation of calcite takes place between 650 and 950 °C whereas aragonite and vaterite dissociate between 530 and 650 °C.

Fig. 16 presents the thermogravimetric (TGA) and derivative thermogravimetric (DTG) profiles of each mortar series at different healing periods. From the DTG profiles, two predominant peaks can be observed for $CaCO_3$ in the range of 580 to 900 °C. These two peaks correspond to aragonite/vaterite at (580–780 °C) and calcite at (780–900 °C). In the CTRL series, the peaks of calcite (Ca) were not that pronounced compared to aragonite/vaterite (Ar/Vr) peaks at 28- and 56-days healing. However, for bacteria containing series, both peaks of calcite and aragonite/vaterite were clearly prominent in the DTG profiles.

To differentiate the self-healing performance between each mortar series at different healing periods, mass percentage of $CaCO_3$ was calculated using the TGA profiles and Equation (6) at each healing period. From Fig. 16, it was reported that the increase in the mass % of $CaCO_3$ was only reported for CTRL and AKD5.0 as the healing period increased. In the CTRL series the mass % of $CaCO_3$ was reported to be 3.74% (0.75% Ca and 2.99% Ar/Vr) which increased to 4.06% (0.79% Ca and 3.27% Ar/Vr) at 56 days of healing. Thus, using Equation (7), a self-healing efficiency of only 8.55% in terms of increase amount of $CaCO_3$ was reported in CTRL series from 28 to 56 days healing. Meanwhile in the AKD5.0 series, the mass % of $CaCO_3$ obtained was 4.86% (1.38% Ca and 3.48% Ar/Vr) at 28 days healing. After 56 days healing, the final mass % of $CaCO_3$ was 5.44% (1.55% Ca and 3.89% Ar/Vr) which led to a self-healing efficiency of 12%. In the case of PLA series and AKD2.6, a decrease in the mass % of $CaCO_3$ was observed beyond the 28 days of healing. The mass % of $CaCO_3$ at 28 days of healing for PLA2.6, PLA5.0 and AKD2.6 were 5.16%, 6.1% and 5.62%, respectively. This implies that PLA at 5% dosage had the best self-healing performance at 28 days healing. Nevertheless at 56 days of healing, the mass % of $CaCO_3$ decreased to 5.02%, 5.45% and 4.76% for PLA2.6, PLA5.0 and AKD2.6, respectively. Hence a decrease in the self-healing performance was reported for the above-mentioned series after 56 days of healing.

4. Discussion

4.1. Effect of healing duration on self-healing capacity

From the results obtained from the stereomicroscopic observations and the rapid water permeability test, the crack width and the water flowing through these cracks reduced as the healing period increased. Moreover, at higher healing periods (56 days healing), the crack healing capacity obtained was comparatively higher than the ones obtained at 28 days of healing for the mortar series especially for the healing agent added series. In addition, a complete crack closure was achieved at 56 days of healing for the mortar series at different initial crack widths and was more frequent (five times in PLA5.0 out of 12 samples, three times in AKD5.0 out of 9 samples and only one time in CTRL out of 9 samples) for the bacterial containing series. In terms of recovery of water tightness at 56 days of healing, the self-healing capacity increased from its 28 days healing period for all the mortar series. This can be accounted to two following reasons. According to Huang et al. [51], a small amount of unhydrated cement particles was present inside the crack and due to a relatively prolonged amount of water exposure after 56 days of healing, the resulting water-to-cement ratio inside the crack was very high. This led to accelerated hydration and thus an enhanced formation of healing products in the crack mouth leading to autogenous healing. Another reason stated by Tziviloglou et al. [27] was the more availability of carbonates in the water and exposure to oxygen with increased healing period, thus promoting bacterial activity leading to the increased production of $CaCO_3$ (autonomous healing). Besides, the crack healing capacity at the BF was comparatively lower than the TF because it was hypothesized that the amount of dissolved oxygen concentration is less at higher depths since most of the dissolved oxygen is available at the water surface due to diffusion [52].

4.2. Effect of crack width on self-healing capacity

The stereomicroscopic observations revealed that for smaller crack widths ranging between 0.2 and 0.4 mm, the frequency of obtaining higher crack healing capacity was more (100% self-healing achieved for total of nine times out of 20 samples within the same crack width range) compared to the larger crack widths greater than 0.4 mm (100% self-healing achieved for total of three times out of 27 samples with crack widths greater than 0.4 mm). In the case of smaller crack widths both autogenous and autonomous self-healing played a significant role in crack healing. However, in the case of larger crack widths, only autonomous healing was prominent because according to the literature, a complete crack closure in fresh water was achievable only up to 0.2 mm by autogenous healing [7]. Hence to enhance the autogenous healing, bacteria mediated self-healing was introduced which completely healed a crack width of 0.63 mm by the AKD2.6 series. Similarly, in the case of recovery of water tightness, the frequency of obtaining higher self-healing efficiency was more evident for smaller crack widths. However, for an initial crack width of 0.63 mm, AKD2.6 reported its best recovery of water tightness. This can be explained due to the fact of the tortuosity and the roughness of the cracks which may hinder the degree of self-healing as stated by Shin et al. [53].

4.3. Effect of healing agent dosage on self-healing capacity

According to the average self-healing capacity obtained from the stereomicroscopic observations and the water permeability test, healing agents at 5% dosage had reported the best average self-healing capacity for PLA and AKD in comparison to 2.6% dosage. A possible explanation can be the increased concentration of the organic substrate (calcium lactate in PLA and alkanoate copolymer in AKD) results in more production of CO_2 and $CaCO_3$ governed by reaction mechanisms explained in the Introduction section. Similar inferences were obtained by De Belie et al. [54], in which increasing the organic carbon substrate concentration (Ca^{2+} and CO_3^{2-} ions) directly resulted in higher yield of $CaCO_3$.

4.4. Effect of healing duration on variability of crack width and water flow

The variability results from the statistical analysis revealed that for increasing healing period, the variation in the crack widths increased. Similarly, in the case of water flow through the cracks at higher healing periods exhibited huge values of COV in comparison to water flow variation before healing. Two possible explanations can be given for such outcomes:

(1) The degree of self-healing is unequal between different specimens of mortar mixture due to varying internal microstructure and crack geometry. In addition, according to Rossi et al. [37] the distribution and the composition of the healing agent particle might be non-uniform since these healing agent particles are added during the mixing process which might lead to non-uniform self-healing in the crack mouth.
(2) As the healing period increases, the crack walls come more closer in contact with the amount of water flowing through these cracks. Hence the influence of internal geometry of the crack becomes more pronounced on the flow of water through the cracks. A similar inference was reported by Mullem et al. [45] in the variation of water permeability results of self-healing concrete.

4.5. Inconsistency in self-healing capacity from various experimental techniques

The crack-healing capacity from the stereomicroscopic observations reported that for PLA5.0 and AKD5.0, a complete crack closure was reported for a crack width of 0.3 and 0.34 mm, respectively thus, accounting to 100% self-healing. However, the results from the rapid water permeability test reported only 91% and 82% self-healing efficiency for the same effective crack widths. One possible explanation can be accounted to the test conditions adopted for the permeability test. In this test, the same specimens undergone repeated water permeability test to evaluate the performance at 28- and 56-days healing which might lead to flushing out of the components from the crack mouth which are responsible for self-healing. Another possible explanation to this phenomenon can be accounted due to the presence of layer of calcium carbonates on the crack surface which are not enough resistant to a continuous pressure coming from the water column leading to leakage of water through these cracks.

4.6. Evaluation of the $CaCO_3$ precipitation by healing agents

From the XRD results, strong peaks of calcite, aragonite and vaterite for the bacterial containing specimens indicated the influence of microbial induced calcium carbonate precipitation. Besides for PLA2.6 and PLA5.0, the crack width investigated for the XRD analysis was greater than 0.5 mm, indicating a strong influence of the autonomous healing by the healing agents. Moreover, the larger crystallite sizes of the calcium carbonate in the bacteria containing series compared to the CTRL series displayed a stronger influence of the autonomous healing especially for larger crack widths. Thus, confirming that majority of these crystals are produced by the healing agents.

In the TGA analysis, less mass % of $CaCO_3$ was reported for the PLA and AKD2.6 series after 56 days of healing. As the healing period increases, the alkalinity of the matrix increases due to the production of lime (cement hydration) [55]. In the case of PLA series, the high alkalinity of the matrix after 56 days of healing may possess limited compatibilities. After 56 days of complete immersion, the Ca^{2+} ions in the pore solution decreases due to the formation of calcium carbonate precipitation by bacteria. This leads to dissolution of hydration products such as lime (leaching of calcium ions) which causes an increase in the pore volume, resulting in the loss of $CaCO_3$ precipitate formed in the smaller pores prior to 56 days of healing [37]. However, in AKD series, the healing agents are more compatible in high alkaline environment, since the $CaCO_3$ precipitates formed in the pores are lesser in comparison to PLA (which also acts as a source of Ca^{2+} ions) series. This leads to an optimum concentration of calcium ions in pore solution which promotes the stability of lime [40]. Hence in the case of AKD2.6, the diminishing self-healing effect could be attributed to the lack of alkanoates present to precipitate the required $CaCO_3$ at 56 days of healing.

5. Conclusions

In this study, an alternative non-toxic biodegradable bioplastic healing agent, to the already-developed healing agents made of lactic acid derivatives (PLA) were investigated for the self-healing efficiency of the mortar specimens. The self-healing by these alternative healing agents known as alkanoate derivatives (AKD) in the mortar specimens were quantified and characterized and the following major conclusions were drawn:

- The average self-healing capacity in terms of crack sealing and recovery of water tightness were highest for PLA5.0 and AKD5.0.

- The maximum completely healed crack width corresponded to 0.63 mm by AKD2.6, followed by PLA5.0 of crack widths corresponded to 0.55 and 0.52 mm.
- A complete crack closure was observed for all the mortar series in the crack widths ranging from 0.28 to 0.4 mm. CTRL, PLA2.6, PLA5.0, AKD2.6 and AKD5.0 achieved a complete crack closure at an initial effective crack width of 0.28 mm, 0.36 mm, 0.36 mm, 0.36 mm and 0.39 mm, respectively.
- PLA5.0 achieved five times complete crack closure, followed by AKD5.0 at three times, AKD2.6 at two times and CTRL, PLA2.6 one time each for different initial effective crack widths.
- Stereomicroscopic images displayed a complete filling of the cracks for the bacteria containing series at 56 days healing.
- In the CTRL series, 97% recovery of water tightness was obtained for an initial crack width of 0.28 mm. In the bacteria containing series, AKD2.6 reported the best recovery of water tightness of 95% at a crack width of 0.63 mm followed by PLA5.0 with a recovery of water tightness corresponding to 91% at a crack width of 0.30 mm.
- Variation of the crack width and water flow increased at higher healing periods due to the influence of internal crack geometry.
- Indication of calcium carbonate precipitation by the healing agents were confirmed by the XRD and TGA analysis. In TGA analysis, the mass % of $CaCO_3$ increased in the PLA and AKD2.6 only up to 28 days healing period whereas in AKD5.0 and CTRL, the mass % of $CaCO_3$ increased up to 56 days healing period.

Funding

This research received no external funding.

CRediT authorship contribution statement

Rahul Roy: Conceptualization, Methodology, Validation, Investigation, Visualization, Writing - original draft. **Emanuele Rossi:** Data curation, Formal analysis, Writing - review & editing, Supervision. **Johan Silfwerbrand:** Resources, Supervision. **Henk Jonkers:** Resources, Supervision, Project administration.

Declaration of Competing Interest

The authors declare that they have no known competing financial interests or personal relationships that could have appeared to influence the work reported in this paper.

Acknowledgments

The authors would like to thank Arjan Thijssen for his assistance with the X-ray diffraction analysis and John van den Berg for his assistance with the Thermogravimetric analysis. Special thanks to Erik Schlangen for providing the opportunity to conduct this project.

References

[1] H.G. Van Oss, Background facts and issues concerning cement and cement data, US Geological Survey Open-File Report 1152 (2005) 88.
[2] B. Han, L. Zhang, J. Ou, Smart and Multifunctional Concrete Toward Sustainable Infrastructures, Singapore: Springer Singapore Pte. Limited, Singapore, 2017.
[3] K. Breugel. Is there a market for self-healing cement-based materials? 2007.
[4] C. Dry, Matrix cracking repair and filling using active and passive modes for smart timed release of chemicals from fibers into cement matrices, Smart Mater. Struct. 3 (2) (1994) 118–123.
[5] B. Han et al., Smart concretes and structures: a review, J. Intel. Mater. Systems Struct. 26 (11) (2015) 1303–1345.
[6] K. Van Tittelboom, N. De Belie, Self-healing in cementitious materials—a review, Materials 6 (6) (2013) 2182–2217.
[7] T. Danner, U. Hjorth Jakobsen, M.R. Geiker, Mineralogical sequence of self-healing products in cracked marine concrete, Minerals 9 (5) (2019).
[8] V.S. Ramachandran, *Concrete* Admixtures Handbook: Properties, Science and Technology, William Andrew, 1996.
[9] H.M. Jonkers, Self healing concrete: a biological approach, in Self Healing Materials: An Alternative Approach to 20 Centuries of Materials Science, S. van der Zwaag, 2007, Springer Netherlands: Dordrecht. p. 195-204.
[10] P. Ghosh et al., Development of bioconcrete material using an enrichment culture of novel thermophilic anaerobic bacteria, Indian J. Exp. Biol. 44 (4) (2006) 336–339.
[11] H.M. Jonkers et al., Application of bacteria as self-healing agent for the development of sustainable concrete, Ecol. Eng. 36 (2) (2010) 230–235.
[12] K. Van Tittelboom et al., Use of bacteria to repair cracks in concrete, Cem. Concr. Res. 40 (1) (2010) 157–166.
[13] R. Siddique, N.K. Chahal, Effect of ureolytic bacteria on concrete properties, Constr. Build. Mater. 25 (10) (2011) 3791–3801.
[14] M. Seifan, A.K. Samani, A. Berenjian, Bioconcrete: next generation of self-healing concrete, Appl. Microbiol. Biotechnol. 100 (6) (2016) 2591–2602.
[15] H. Jonkers et al., Biotech Solutions for Concrete Repair with Enhanced Durability, Elsevier, 2016, p. 1.
[16] H.M. Jonkers, Bacteria-based self-healing concrete, Heron 56 (1/2) (2011).
[17] J. Wang et al., Application of hydrogel encapsulated carbonate precipitating bacteria for approaching a realistic self-healing in concrete, Constr. Build. Mater. 68 (2014) 110–119.
[18] G. Trenson, Application of pH responsive hydrogel encapsulated bacteria. 2017.
[19] J. Wang et al., A chitosan based pH-responsive hydrogel for encapsulation of bacteria for self-sealing concrete, Cem. Concr. Compos. 93 (2018) 309–322.
[20] S. Shahid et al., Self-healing of cracks in concrete using bacillus strains encapsulated in sodium alginate beads, ChemistrySelect 5 (1) (2020) 312–323.
[21] D. Palin, V. Wiktor, H.M. Jonkers, A bacteria-based self-healing cementitious composite for application in low-temperature marine environments, Biomimetics 2 (3) (2017) 13.
[22] J. Wang et al., Use of silica gel or polyurethane immobilized bacteria for self-healing concrete, Constr. Build. Mater. 26 (1) (2012) 532–540.
[23] J. Wang et al., Self-healing concrete by use of microencapsulated bacterial spores, Cem. Concr. Res. 56 (2014) 139–152.
[24] H. Xu et al., Self-healing concrete using rubber particles to immobilize bacterial spores, Materials 12 (14) (2019) 2313.
[25] N.H. Balam, D. Mostofinejad, M. Eftekhar, Effects of bacterial remediation on compressive strength, water absorption, and chloride permeability of lightweight aggregate concrete, Constr. Build. Mater. 145 (2017) 107–116.
[26] W. Khaliq, M.B. Ehsan, Crack healing in concrete using various bio influenced self-healing techniques, Constr. Build. Mater. 102 (2016) 349–357.
[27] E. Tziviloglou et al., Bacteria-based self-healing concrete to increase liquid tightness of cracks, Constr. Build. Mater. 122 (2016) 118–125.
[28] Y.Ç. Erşan et al., Enhanced crack closure performance of microbial mortar through nitrate reduction, Cem. Concr. Compos. 70 (2016) 159–170.
[29] V. Wiktor, H.M. Jonkers, Quantification of crack-healing in novel bacteria-based self-healing concrete, Cem. Concr. Compos. 33 (7) (2011) 763–770.
[30] N.N.T. Huynh et al., Bacillus subtilis HU58 Immobilized in micropores of diatomite for using in self-healing concrete, Proc. Eng. 171 (2017) 598–605.
[31] J.-Y. Wang, N. De Belie, W. Verstraete, Diatomaceous earth as a protective vehicle for bacteria applied for self-healing concrete, J. Ind. Microbiol. Biotechnol. 39 (4) (2012) 567–577.
[32] S. Gupta, H.W. Kua, S. Dai Pang, Healing cement mortar by immobilization of bacteria in biochar: an integrated approach of self-healing and carbon sequestration, Cem. Concr. Compos. 86 (2018) 238–254.
[33] H.W. Kua et al., Biochar-immobilized bacteria and superabsorbent polymers enable self-healing of fiber-reinforced concrete after multiple damage cycles, Cem. Concr. Compos. 100 (2019) 35–52.
[34] R.M. Mors, H.M. Jonkers, Reduction of water permeation through cracks in mortar by addition of bacteria based healing agent. 2015.
[35] R.M. Mors, H.M. Jonkers, Feasibility of lactate derivative based agent as additive for concrete for regain of crack water tightness by bacterial metabolism, Industrial Crops Prod. 106 (2017) 97–104.
[36] C.R. Rodríguez et al., Chemo-physico-mechanical properties of the interface zone between bacterial PLA self-healing capsules and cement paste, Cem. Concr. Res. 138 (2020) 106228.
[37] E. Rossi et al., On the applicability of a precursor derived from organic waste streams for bacteria-based self-healing concrete, Front. Built Environ. 7 (2) (2021).
[38] V. Stabnikov, V. Ivanov, J. Chu, Construction Biotechnology: a new area of biotechnological research and applications, World J Microbiol Biotechnol 31 (9) (2015) 1303–1314.
[39] V. Stabnikov, V. Ivanov, 3 - Biotechnological Production of Biopolymers and Admixtures for Eco-efficient Construction Materials, Elsevier Ltd., 2016, pp. 37–56.
[40] C.M. Vermeer et al., From waste to self-healing concrete: a proof-of-concept of a new application for polyhydroxyalkanoate, Resour. Conserv. Recycling 164 (2021).
[41] R. Rahul et al., Encapsulation techniques and test methods of evaluating the bacteria-based self-healing efficiency of concrete: a literature review, Nordic Concr. Res. 62 (1) (2020) 63–85.
[42] M. Magalla, Bacteria based self-healing concrete. 2017.

[43] D. Palin, H. Jonkers, V. Wiktor, Autogenous healing of sea-water exposed mortar: quantification through a simple and rapid permeability test, Cem. Concr. Res. 84 (2016) 1–7.
[44] C. Edvardsen, Water permeability and autogenous healing of cracks in concrete, in: Innovation in Concrete Structures: Design and Construction, Thomas Telford Publishing487, 1999, p. 473.
[45] T. Van Mullem et al., Novel active crack width control technique to reduce the variation on water permeability results for self-healing concrete, Constr. Build. Mater. 203 (2019) 541–551.
[46] A.K. Zak et al., X-ray analysis of ZnO nanoparticles by Williamson-Hall and size–strain plot methods, Solid State Sci. 13 (1) (2011) 251–256.
[47] M. Ksara et al., Microbial damage mitigation strategy in cementitious materials exposed to calcium chloride, Constr. Build. Mater. 195 (2019) 1–9.
[48] M.D. Hager, S. Van der Zwaag, U.S. Schubert, Self-healing Materials, Springer, 2016.
[49] S. Gopi, V. Subramanian, K. Palanisamy, Aragonite–calcite–vaterite: A temperature influenced sequential polymorphic transformation of CaCO3 in the presence of DTPA, Mater. Res. Bull. 48 (5) (2013) 1906–1912.
[50] G. Villain, M. Thiery, G. Platret, Measurement methods of carbonation profiles in concrete: thermogravimetry, chemical analysis and gammadensimetry, Cem. Concr. Res. 37 (8) (2007) 1182–1192.
[51] H. Huang, G. Ye, D. Damidot, Characterization and quantification of self-healing behaviors of microcracks due to further hydration in cement paste, Cem. Concr. Res. 52 (2013) 71–81.
[52] J.J. Childress, B.A. Seibel, Life at stable low oxygen levels: adaptations of animals to oceanic oxygen minimum layers, J. Exp. Biol. 201 (Pt 8) (1998) 1223–1232.
[53] K.J. Shin et al., Parameters influencing water permeability coefficient of cracked concrete specimens, Constr. Build. Mater. 151 (2017) 907–915.
[54] N. De Belie, 19 - Bacteria-based concrete, Woodhead Publishing, 2018, pp. 531–567.
[55] P. Šiler et al., The determination of the influence of pH value of curing conditions on Portland cement hydration, Proc. Eng. 151 (2016) 10–17.
[56] T. Van Mullem et al., First large scale application with self-healing concrete in Belgium: analysis of the laboratory control tests, Materials 13 (4) (2020) 997.
[57] Y.Ç. Erşan et al., Self-protected nitrate reducing culture for intrinsic repair of concrete cracks, Front. Microbiol. 6 (1228) (2015).